Supporting Information for

Nitrosyl Linkage Isomers: NO Coupling to N_2O at a Mononuclear Site

Subrata Kundu,[1,2] Phan N. Phu,[3] Pokhraj Ghosh,[1] Stosh A. Kozimor,[4] Jeffery A. Bertke,[1] S. Chantal E. Stieber,[3,4,*] and Timothy H. Warren[1,*]

[1] Department of Chemistry, Georgetown University, Box 571227, Washington, DC 20057-1227, United States.

[2] School of Chemistry, Indian Institute of Science Education and Research Thiruvananthapuram, Kerala 695551, India.

[3] California State Polytechnic University, Pomona, California 91768, United States.

[4] Los Alamos National Laboratory, Los Alamos, New Mexico 87545, United States.

*Corresponding author emails: sestieber@cpp.edu (S.C.E.S), thw@georgetown.edu (T.H.W)

Table of Contents

1. General Instrumentation and Physical Methods.

The preparation and handling of air-sensitive chemicals were done under dry nitrogen atmosphere by utilizing MBraun gloveboxes and/or standard Schlenk techniques unless otherwise mentioned. ^{1}H, ^{13}C, and ^{19}F NMR spectra were recorded on a Varian 400 MHz spectrometer at room temperature unless otherwise noted. The chemical shift (δ) values are expressed in ppm relative to tetramethylsilane, whereas the residual ^{1}H signal of deuterated solvent served as an internal standard. ^{19}F NMR spectra were recorded in presence of an internal reference of C_6F_6 (δ = -164.90 ppm). ^{15}N NMR spectra were recorded at 41.0 MHz and referenced to external standard $Na^{15}NO_2$ in D_2O (609.5 ppm *vs.* liquid NH_3). Elemental analyses were performed on a Perkin-Elmer PE2400 micro-analyzer at Georgetown University. UV-vis spectra were recorded on Agilent 8454 Diode Array spectrometer equipped with stirrer and Unisoku USP-203 cryostat for variable temperature (-105 °C to 90 °C) experiments. The molar extinction coefficients of different isolated complexes were determined from Beer's law plots (absorbance *vs* concentration) with at least four different concentrations. IR spectra (with spectral resolution of 2 cm^{-1}) were collected on a Varian 3100 FT-IR spectrometer by using KBr pellet method unless otherwise mentioned. Solution IR spectra were recorded using a Mettler Toledo ReactIR spectrometer equipped with optical fiber probe with diamond ATR and MCT detector. Cyclic voltammetry measurements were done at room temperature under dry nitrogen atmosphere of a glove-box using BASi Epsilon Electrochemistry setup with three electrodes (Working electrode: glassy carbon, Auxiliary electrode: platinum wire, Pseudo-reference electrode: silver wire). Details for EPR spectra and X-ray crystallography appear in Sections 10 and 11, respectively.

2. Materials.

All chemicals were purchased from common vendors (e.g. Sigma-Aldrich, Acros Organics, Strem Chemicals, TCI) and used without further purification unless otherwise mentioned. Potassium graphite (KC_8) was obtained from Strem Chemicals. Molecular sieves (4A, 4-8 mesh beads) were obtained from Fisher Scientific and activated *in vacuo* at 180 °C for 24 h. Extra dry solvents (≥99.5%) with Acroseal® and deuterated solvents were purchased from Acros Organics and Cambridge Isotope Laboratories, respectively. Both anhydrous and deuterated solvents were sparged with nitrogen and stored over activated 4A molecular sieves under a nitrogen atmosphere. Nitric oxide gas (unlabeled) was obtained from Praxair and purified by passing through a column of Ascarite (8-20 mesh) purchased from Sigma. ^{15}N labelled nitric oxide (^{15}N, 98%+) was procured from Cambridge Isotope Laboratories.

The nickel-nitrosyl precursor[1] $Ni(NO)I(THF)_2$ and $H[^{i}Pr_2NN_{F6}]$[2] were synthesized and characterized according to literature procedures. $Ni(^{15}NO)I(THF)_2$ was prepared by using ^{15}N-nitric oxide (98+% ^{15}N) instead of naturally abundant nitric oxide.

3. Synthesis and characterization of [^{i}Pr$_2$NN$_{F6}$]NiNO (1).

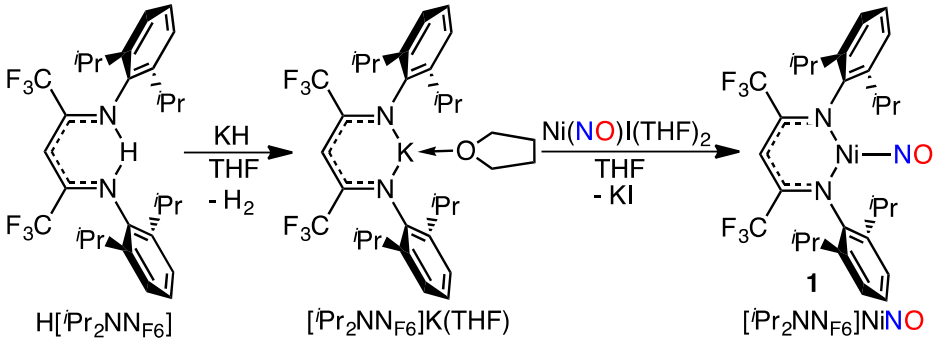

Scheme S1. Synthesis of [^{i}Pr$_2$NN$_{F6}$]NiNO (**1**).

A two-step synthesis (Scheme S1) was employed. Step 1: Solid KH (0.195 g, 4.855 mmol) was slowly added to a vigorously stirring solution of H[^{i}Pr$_2$NN$_{F6}$] (2.132 g, 4.049 mmol) in tetrahydrofuran (15 mL). Evolution of hydrogen gas was observed and the reaction mixture was allowed to stir overnight at room temperature. The resultant reaction mixture was filtered and the dark yellow filtrate was evaporated under reduced pressure to obtain a concentrated solution. Pentane (15 mL) was added to the concentrated solution to obtain a yellow precipitate, which was isolated by filtration and dried under vacuum to afford the potassium salt of the ligand [^{i}Pr$_2$NN$_{F6}$]K(THF) as yellow solid in near quantitative yield (2.561 g, 4.023 mmol). ^{1}H NMR (400 MHz, CD_3CN): δ 6.84 (d, 4H, *m*-Ar-*H*), 6.73 (t, 2H, *p*-Ar-*H*), 3.65 (m, 4H, THF-CH_2), 3.18 (s, 1H, backbone-C*H*), 2.80 (sep, 4H, -C*H*Me$_2$), 1.82 (m, 4H, THF-CH_2), 0.97 (d, 12H, -CH*Me*$_2$), 0.83 (d, 12H, -CH*Me*$_2$). ^{13}C{^{1}H} NMR (100 MHz, CD_3CN): δ 153.77, 149.48, 138.95, 123.37, 122.98 (q, $^{1}J_{CF}$ = 280 Hz), 121.96, 79.10, 68.30, 28.14, 26.26, 23.98, 23.81. ^{19}F NMR (376 MHz, CD_3CN): δ -66.54 (s, -CF_3).

Step 2: A solution of Ni(NO)I(THF)$_2$ (1.440 g, 4.025 mmol) in anhydrous tetrahydrofuran (5 mL) was added to a solution of [^{i}Pr$_2$NN$_{F6}$]K(THF) (2.561 g, 4.023 mmol) in tetrahydrofuran (5 mL). The resultant reaction mixture was stirred at room temperature for 3 h. Then the reaction mixture was filtered through celite and the green filtrate thus obtained was evaporated under reduced pressure to afford a green powder. The crude product was further dissolved in pentane and filtered to remove any unreacted starting material. The filtrate thus obtained was evaporated to afford the desired product as microcrystalline green powder (1.882 g, 3.063 mmol) in 76% yield of **1**. X-ray quality crystals were grown by slow evaporation of a concentrated heptane solution of **1** at room temperature. Anal. Calcd for

$C_{29}H_{35}F_6N_3NiO$: C, 56.70; H, 5.74; N, 6.84. Found: C, 56.36; H, 6.10; N, 6.78. UV-Vis (THF, 25 °C): λ_{max}/nm (ε/$M^{-1}cm^{-1}$) = 615 (150). ^1H NMR (400 MHz, C_6D_6): δ 7.18 (m, 2H, *p*-Ar-*H*), 7.08-7.12 (m, 4H, *m*-Ar-*H*), 5.59 (s, 1H, backbone-C*H*), 3.39 (sep, 4H, -C*H*Me_2), 1.47 (d, 12H, -CH*Me*$_2$), 1.29 (d, 12H, -CH*Me*$_2$). $^{13}C\{^1H\}$ NMR (100 MHz, 298 K, C_6D_6): δ 150.61 (q, $^2J_{CF}$ = 27.1 Hz), 147.76, 141.45, 127.61, 123.83, 121.11 (q, $^1J_{CF}$ = 285.3 Hz), 85.61 (m, $^3J_{CF}$ = 5.0 Hz), 29.37, 25.37, 22.88. ^{19}F NMR (376 MHz, C_6D_6): δ -64.54 (s, -C*F*$_3$). FT-IR (KBr pellet, cm^{-1}): 1825 [ν(^{14}NO)].

^{15}N-labelled complex **1**-^{15}N was synthesized by employing Ni(^{15}NO)I(THF)$_2$. A sample for ^{15}N NMR was prepared by dissolving *ca.* 60 mg of **1**-^{15}N in C_6D_6 (*ca.* 0.6 mL). ^{15}N NMR (41 MHz, C_6D_6): δ 377.89 (*vs* liquid NH_3). FT-IR (KBr pellet, cm^{-1}): 1787 [ν(^{15}NO)]. The observed $^{15}N/^{14}N$-shift for the isotope sensitive band at 1825 cm^{-1} was found to be $^{15N/14N}\Delta\nu$ = 38 cm^{-1} (calculated $^{15N/14N}\Delta\nu$ from Hooke's Law is 38 cm^{-1}).

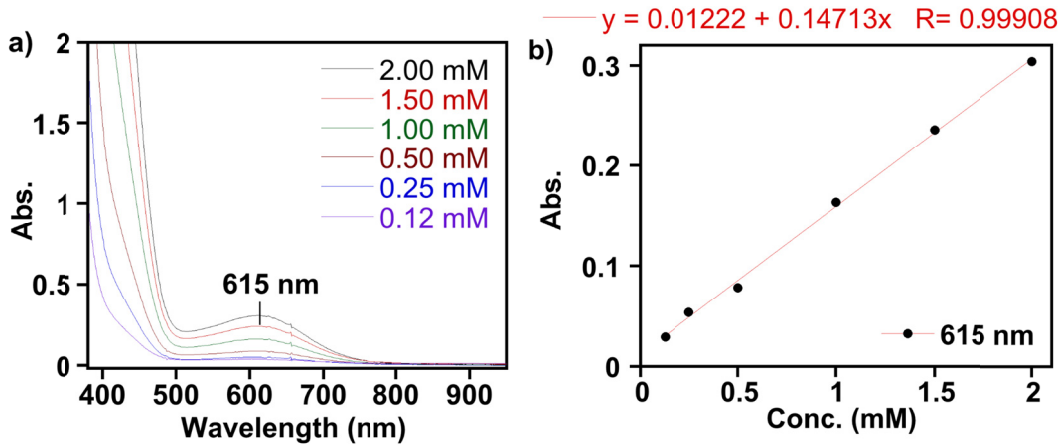

Figure S1. (a) UV-Vis spectra of [^{i}Pr$_2$NN$_{F6}$]NiNO (**1**) in tetrahydrofuran at 25 °C at different concentrations. (b) Beer's law plot for [^{i}Pr$_2$NN$_{F6}$]NiNO (**1**) depicts λ_{max} = 615 nm (ε = 150 $M^{-1}cm^{-1}$).

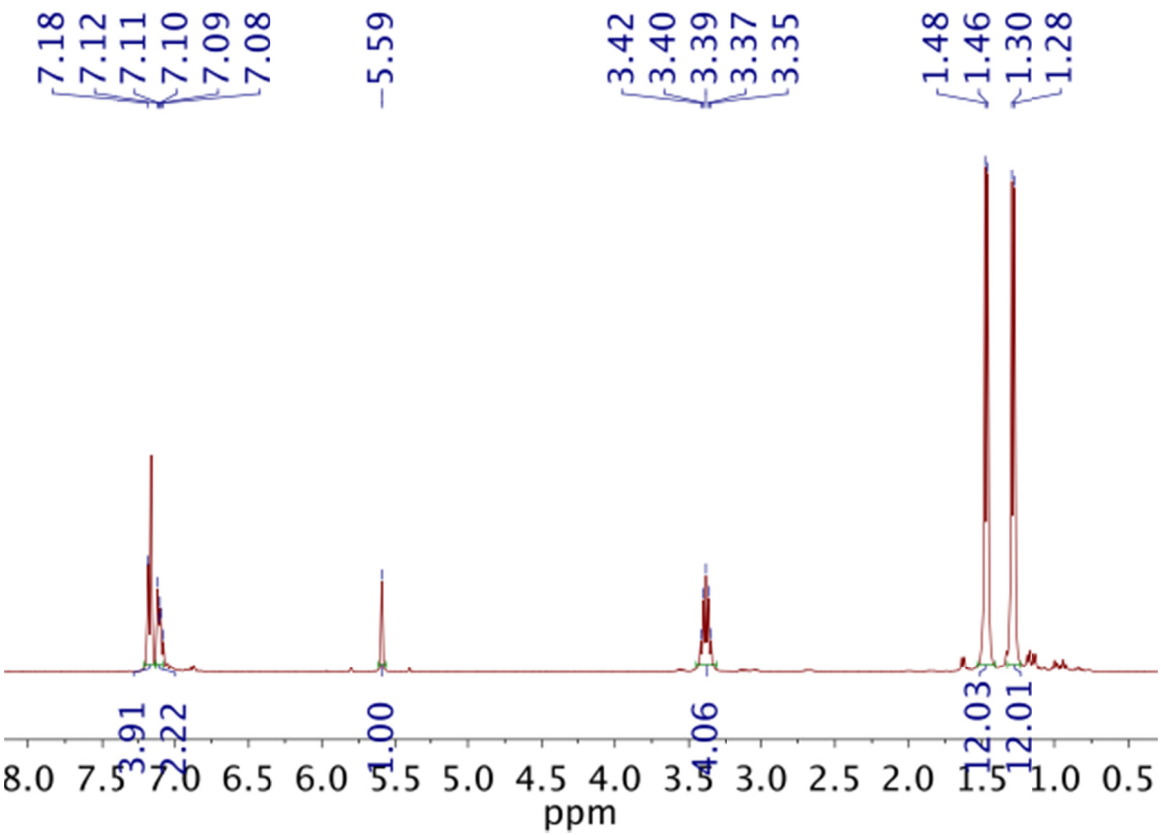

Figure S2. ^{1}H NMR spectrum (399 MHz, 298 K, C_6D_6) of [^{i}Pr$_2$NN$_{F6}$]NiNO (**1**).

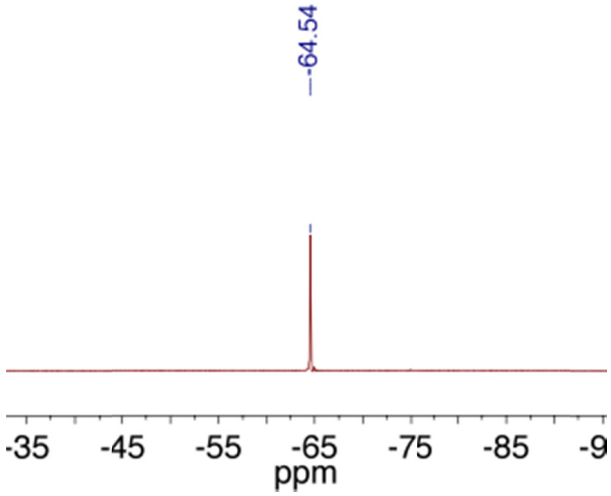

Figure S3. ^{19}F NMR spectrum (376 MHz, 298 K, C_6D_6) of [^{i}Pr$_2$NN$_{F6}$]NiNO (**1**).

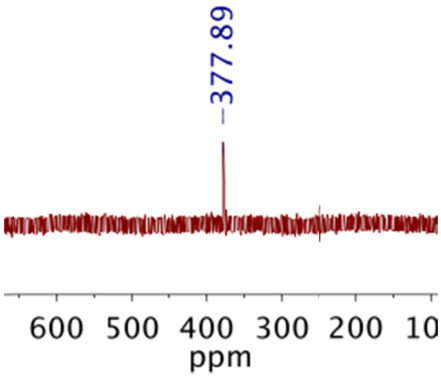

Figure S4. ^{15}N NMR spectrum (41 MHz, 298 K, C_6D_6) of [^{i}Pr$_2$NN$_{F6}$]Ni^{15}NO (**1**-^{15}N).

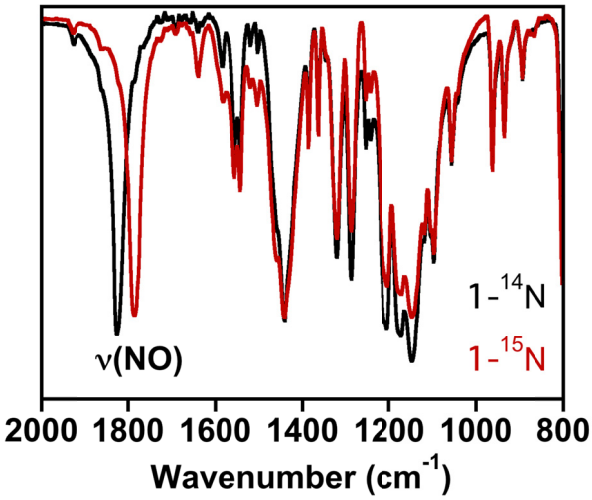

Figure S5. FT-IR (KBr pellet) spectra of [^{i}Pr$_2$NN$_{F6}$]NiNO (**1**) (black trace) and [^{i}Pr$_2$NN$_{F6}$]Ni^{15}NO (**1**-^{15}N) (red trace). The ν(NO) at 1825 cm^{-1} (for **1**) downshifts to 1787 cm^{-1} for ^{15}N enriched sample **1**-^{15}N. Notably, the observed ^{15}N/^{14}N-shift $^{15N/14N}\Delta\nu$ = 38 cm^{-1} is same as predicted from the Hooke's Law calculated shift $^{15N/14N}\Delta\nu$ of 38 cm^{-1}.

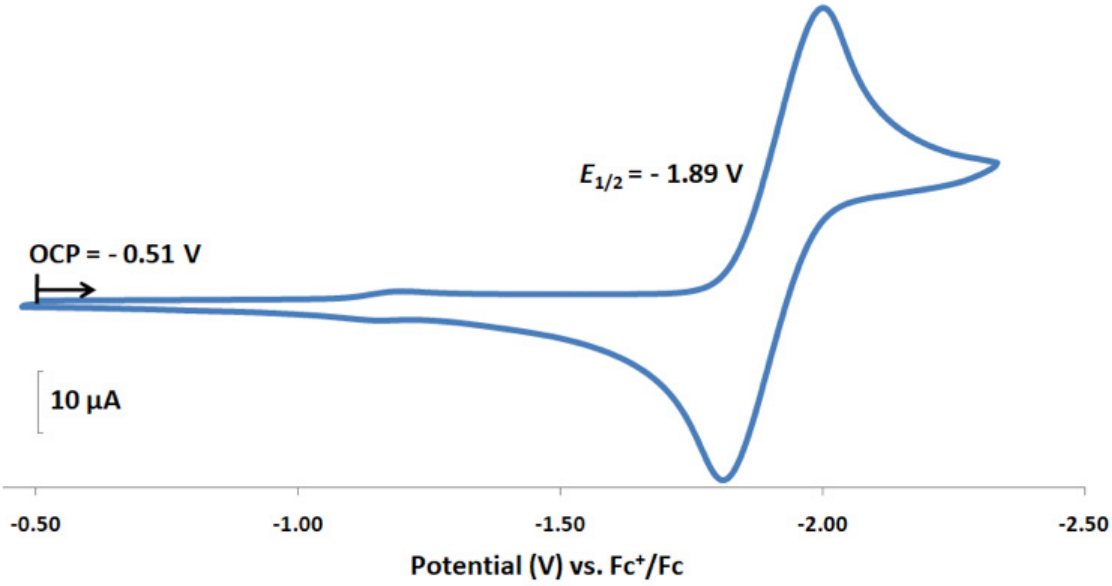

Figure S6. Cyclic voltammogram of [^{i}Pr$_2$NNF$_6$]NiNO (**1**) (4.0 mM in THF at 25 °C) in presence of *n*-tetrabutyl ammonium hexafluorophosphate (0.2 M). Scan proceeds in the indicated direction with scan rate of 50 mV/s. The open circuit potential was -0.51 V vs Fc^{+}/Fc.

4. Synthesis and Characterization of [^{i}Pr$_2$NN$_{F6}$]Ni(μ-η^2:η^2-NO)(K[18-crown-6])(THF) (2a).

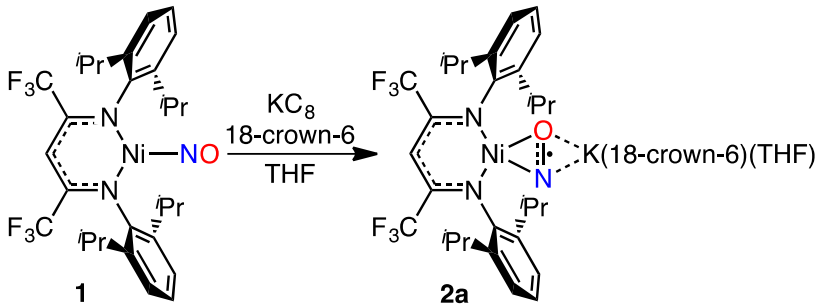

Scheme S2. Synthesis of [^{i}Pr$_2$NN$_{F6}$]Ni(μ-η^2:η^2-NO)K[18-crown-6](THF) (**2a**).

A solution of [^{i}Pr $_2$NN$_{F6}$]NiNO (**1**) (0.364 g, 0.593 mmol) and 18-crown-6 ether (0.157 g, 0.593 mmol) in tetrahydrofuran was added to KC_8 (0.119 g, 0.876 mmol) flakes. After stirring for 30 min, the resultant dark reaction mixture was filtered through celite and a dark purple filtrate was evaporated under reduced pressure to obtain the crude product as a purple solid, which was then washed thoroughly with pentane (*ca.* 15 mL) and dried to afford **2a** as dark purple powder (0.485 g, 0.528 mmol) in 89% yield. A concentrated solution of **2a** in THF/pentane (1:1) at -40 °C afforded X-ray quality crystals. Anal. Calcd for $C_{41}H_{59}F_6N_3NiO_7K$: C, 53.66; H, 6.48; N, 4.58. Found: C, 53.41; H, 6.87; N, 4.32. UV-Vis (THF, 25 °C): λ_{max} = 520 nm (ε = 3050 $M^{-1}cm^{-1}$). FT-IR (KBr pellet, cm^{-1}): 894 [$\nu(^{14}NO)$]. X-band EPR spectra (THF, 293 K): g_{iso} = 2.0008, A_{14N} = 29.1 MHz.

^{15}N-labelled **2a** was synthesized by reduction of **1**-^{15}N using KC_8 in presence of 18-crown-6 as described above. FT-IR (KBr pellet, cm^{-1}): 878 [$\nu(^{15}NO)$]. The observed $^{15}N/^{14}N$-shift for the isotope sensitive band at 894 cm^{-1} was found to be $^{15N/14N}\Delta\nu$ = 16 cm^{-1} (calculated $^{15N/14N}\Delta\nu$ from Hooke's Law is 16 cm^{-1}). EPR spectra (THF, 293 K): g_{iso} = 2.0008, A_{15N} = 40.1 MHz. It is noteworthy that the ratio of isotropic ^{15}N and ^{14}N hyperfine coupling constants $A(^{15}N)/A(^{14}N)$ = 1.34, which is close to the ratio of their gyromagnetic ratios $\gamma(^{15}N)/\gamma(^{14}N)$ = 1.40. Similar correlation between the ratio of ^{15}N / ^{14}N hyperfine coupling constants and the ratio of ^{15}N / ^{14}N gyromagnetic ratios has been previously demonstrated for [^{i}Pr$_2$NN$_{F6}$]Ni(η^2-ONPh) complex.[3]

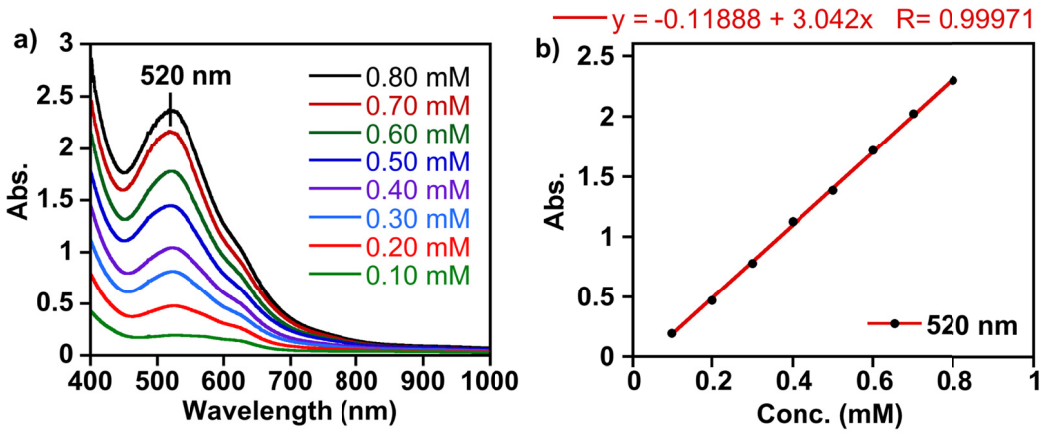

Figure S7. (a) UV-Vis spectra of [^{i}Pr$_2$NN$_{F6}$]Ni(μ-η^2:η^2-NO)K[18-crown-6](THF) (**2a**) in tetrahydrofuran at 25 °C at different concentrations. (b) Beer's law plot for [^{i}Pr$_2$NN$_{F6}$]Ni(μ-η^2:η^2-NO)(K[18-crown-6])(THF) (**2a**) depicts λ_{max} = 520 nm (ε = 3050 M^{-1}cm^{-1}).

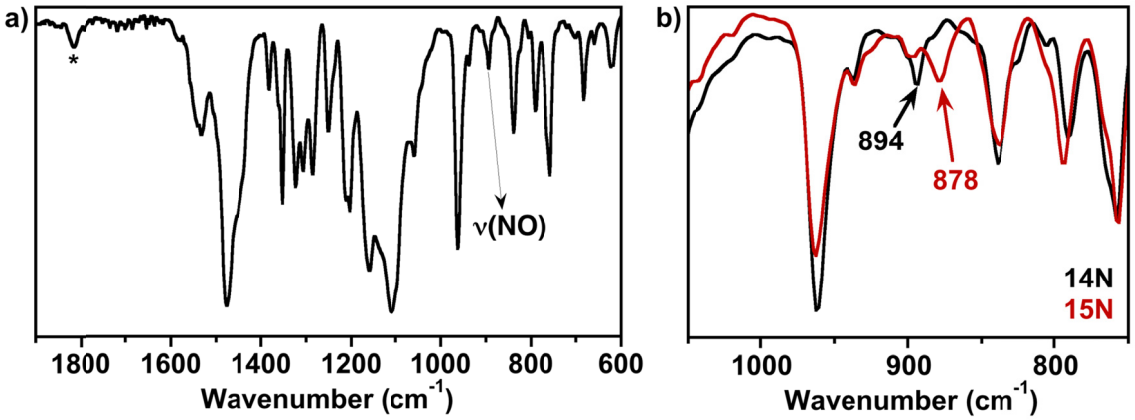

Figure S8. (a) FT-IR (KBr pellet) spectrum of [^{i}Pr$_2$NN$_{F6}$]Ni(μ-η^2:η^2-NO)K[18-crown-6](THF) (**2a**). The vibrational band marked with (*) arises from a trace amount of unreacted [^{i}Pr$_2$NN$_{F6}$]NiNO (**1**). (b) Comparison of FT-IR (KBr pellet) spectra of [^{i}Pr$_2$NN$_{F6}$]Ni(μ-η^2:η^2-NO)(K[18-crown-6])(THF) (**2a**) (black trace) and [^{i}Pr$_2$NN$_{F6}$]Ni(μ-η^2:η^2-^{15}NO)(K[18-crown-6])(THF) (**2a**-^{15}N) (red trace). The ν(NO) at 894 cm^{-1} (for **2a**) downshifts to 878 cm^{-1} for ^{15}N enriched sample **2a**-^{15}N. Notably, the observed ^{15}N/^{14}N-shift $^{15N/14N}\Delta\nu$ = 16 cm^{-1} is same as predicted from the Hooke's Law calculated shift $^{15N/14N}\Delta\nu$ of 16 cm^{-1}.

5. Synthesis and Characterization of [^{i}Pr$_2$NN$_{F6}$]Ni(μ-η^1:η^1-NO)K[2.2.2-cryptand] (2b).

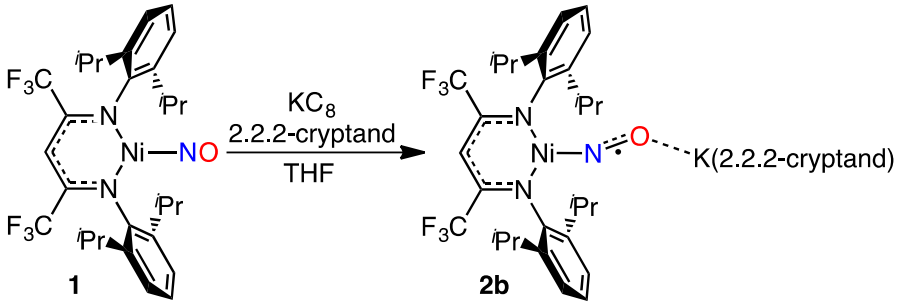

Scheme S3. Synthesis of [^{i}Pr$_2$NN$_{F6}$]Ni(μ-η^1:η^1-NO)K[2.2.2-cryptand] (**2b**).

A solution of [^{i}Pr$_2$NN$_{F6}$]NiNO (**1**) (0.521 g, 0.848 mmol) and 4,7,13,16,21,24-Hexaoxa-1,10-diazabicyclo-[8.8.8]-hexacosane (commonly known as [2.2.2-cryptand]) (0.319 g, 0.848 mmol) in tetrahydrofuran was added to KC_8 (0.180 mg, 1.272 mmol) flakes. After stirring for 30 min, the resultant dark reaction mixture was filtered through celite and a dark purple filtrate was evaporated under reduced pressure to obtain the crude product as a purple solid, which was then washed thoroughly with pentane (*ca.* 20 mL) and dried to afford **2b** as dark brownish purple powder (0.826 g, 0.802 mmol) in 94% yield. A concentrated solution of **2b** in fluorobenzene at -40 °C for overnight afforded X-ray diffraction quality crystals. Anal. Calcd for $C_{51}H_{79}F_6N_5O_8NiK$: C, 55.59; H, 7.23; N, 6.36. Found: C, 55.30; H, 7.58; N, 6.54. UV-Vis (THF, 25 °C): λ_{max} = 495 nm (ε = 1950 $M^{-1}cm^{-1}$). FT-IR (KBr pellet, cm^{-1}): 1555 [$\nu(^{14}NO)$].

^{15}N-labelled **2b** was synthesized by employing **1**-^{15}N and following the above mentioned procedure. FT-IR (KBr pellet, cm^{-1}): 1525 [$\nu(^{15}NO)$]. The observed $^{15}N/^{14}N$-shift for the isotope sensitive band at 1555 cm^{-1} was found to be $^{15N/14N}\Delta\nu$ = 30 cm^{-1} (calculated $^{15N/14N}\Delta\nu$ from Hooke's Law is 31 cm^{-1}).

While the UV-vis spectra of **2a** and **2b** are different (Figures S7 and S9), the UV-vis spectra of **2b** in different solvents and different temperatures did not show any variation in the absorption features of complex **2b**. Moreover, the EPR spectra of **2b** in different solvents at different temperature appear to be similar. Hence, it is not clear whether **2b** in solution exists as endon or sideon or mixture of two isomers.

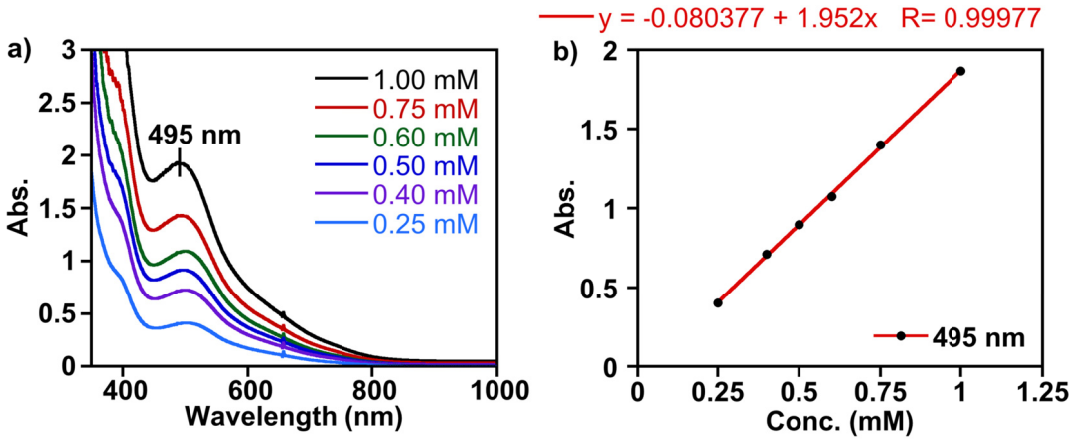

Figure S9. (a) UV-Vis spectra of [^{i}Pr$_2$NN$_{F6}$]Ni(μ-η^1:η^1-NO)K[2.2.2-cryptand] (**2b**) in tetrahydrofuran at 25 ^{o}C at different concentrations. (b) Beer's law plot for [^{i}Pr$_2$NN$_{F6}$]Ni(μ-η^1:η^1-NO)K[2.2.2-cryptand] (**2b**) depicts λ_{max} = 495 nm (ε = 1950 M^{-1}cm^{-1}).

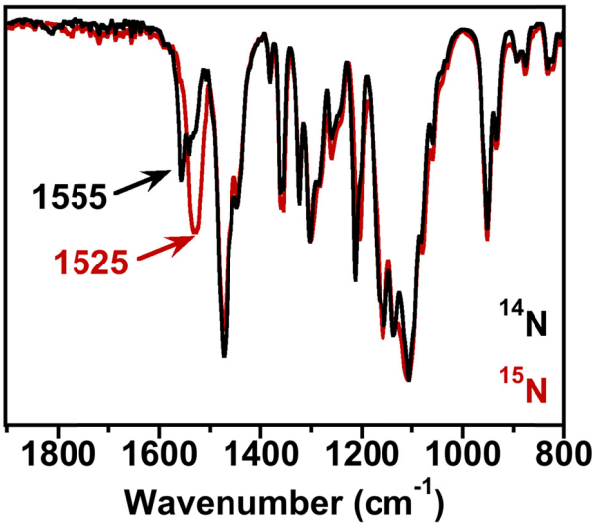

Figure S10. Comparison of FT-IR (KBr pellet) spectra of [^{i}Pr$_2$NN$_{F6}$]Ni(μ-η^1:η^1-NO)K[2.2.2-cryptand] (**2b**) (black trace) and [^{i}Pr$_2$NN$_{F6}$]Ni(μ-η^1:η^1-^{15}NO)K[2.2.2-cryptand] (**2b**-^{15}N) (red trace). The ν(NO) at 1555 cm^{-1} (for **2b**) downshifts to 1525 cm^{-1} for ^{15}N enriched sample **2b**-^{15}N. Notably, the observed ^{15}N/^{14}N-shift $^{15N/14N}\Delta\nu$ = 30 cm^{-1} is same as predicted from the Hooke's Law calculated shift $^{15N/14N}\Delta\nu$ of 29 cm^{-1}.

6. Synthesis and Characterization of [^{i}Pr$_2$NN$_{F6}$]Ni(κ^2-O$_2$N$_2$)K[18-crown-6] (3a).

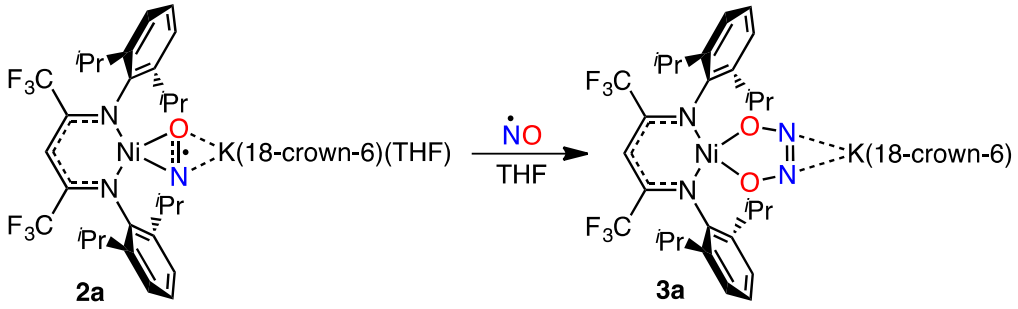

Scheme S4. Synthesis of [^{i}Pr$_2$NN$_{F6}$]Ni(κ^2-O$_2$N$_2$)K[18-crown-6] (**3a**).

A solution of [^{i}Pr$_2$NN$_{F6}$]Ni(μ-η^2:η^2-NO)K[18-crown-6](THF) (**2a**) (0.614 g, 0.621 mmol) in tetrahydrofuran (*ca.* 10 mL) was placed in a Schlenk tube capped with a septum. At room temperature, $NO_{(g)}$ (1 equiv.:15.1 mL, 1.0 atm, 0.621 mmol) was slowly injected to the solution of **2a** and the color of the solution immediately changed from dark purple to brownish red. After stirring 15 min, the resultant solution was evaporated to dryness and the crude product was obtained as brown powder. The crude material was thoroughly washed with pentane (*ca.* 20 mL) and dried to afford a brownish solid **3a** (0.459 g, 0.450 mmol) in 73% yield. Slow evaporation of solvent from a concentrated tetrahydrofuran solution of **3a** at room temperature resulted in X-ray quality crystals. Anal. Calcd for $C_{41}H_{59}F_6N_4NiO_8K$: C, 51.96; H, 6.28; N, 5.91. Found: C, 51.87; H, 6.69; N, 5.62. UV-Vis (THF, 25 °C): λ_{max} = 395 nm (ε = 2860 $M^{-1}cm^{-1}$) and λ_{max} = 550 nm (ε = 780 $M^{-1}cm^{-1}$). ^{1}H NMR (400 MHz, CD_3CN): δ 7.04 (t, 2H, *p*-Ar-*H*), 6.96 (d, 4H, *m*-Ar-*H*), 5.50 (s, 1H, backbone-C*H*), 3.62 (hept, 28H, -C*H*Me$_2$), 3.57 (s, 24H, -C*H*$_2$- from crown ether), 1.48 (d, 12H, -CH*Me*$_2$), 1.23 (d, 12H, -CH*Me*$_2$). ^{13}C{^{1}H} NMR (100 MHz, CD_3CN): δ 148.23 (q, $^2J_{CF}$ = 25.5 Hz), 144.48, 143.28, 129.30, 126.02, 122.91, 120.68 (q, $^1J_{CF}$ = 284.3 Hz), 87.72 (p, $^3J_{CF}$ = 5.8 Hz), 70.89, 29.62, 25.36, 23.32. ^{19}F NMR (376 MHz, CD_3CN): δ -62.22. FT-IR (KBr pellet, cm^{-1}): 1450 [ν(^{14}N^{14}N)].

^{15}N-labelled [^{i}Pr$_2$NN$_{F6}$]Ni(κ^2-O$_2$^{15}N$_2$)K[18-crown-6] (**3a**-^{15}N^{15}N) was prepared from **2a**-^{15}N by addition of 1 equiv. ^{15}NO from a labelled nitric oxide cylinder that was handled inside the glovebox without further purification due to the small amount employed and high cost of ^{15}NO.

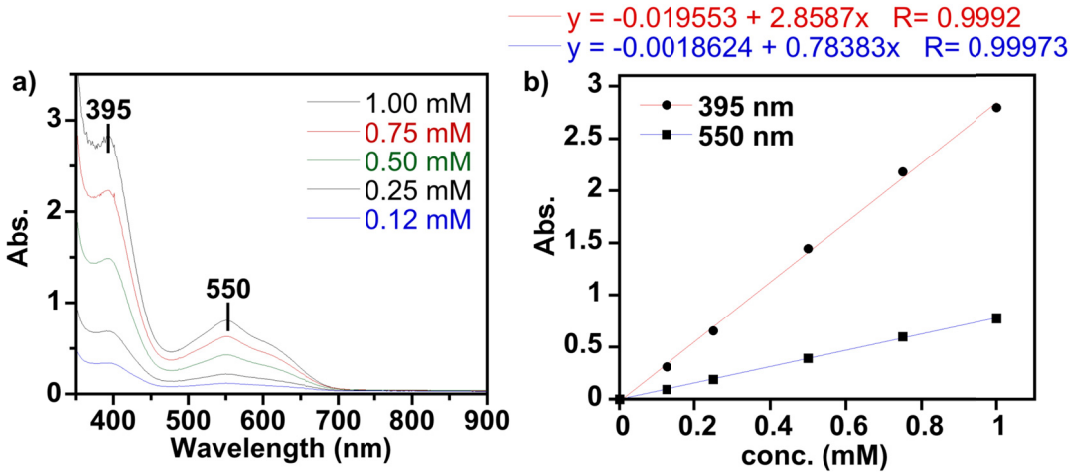

Figure S11. (a) UV-Vis spectra of [^{i}Pr$_2$NN$_{F6}$]Ni(κ^2-O$_2$N$_2$)K(18-crown-6) (**3a**) in tetrahydrofuran at 25 °C at different concentrations. (b) Beer's law plot for [^{i}Pr$_2$NN$_{F6}$]Ni(κ^2-O$_2$N$_2$)K(18-crown-6) (**3a**) depicts λ_{max} = 395 nm (ε = 2860 M^{-1}cm^{-1}) and 550 nm (ε = 780 M^{-1}cm^{-1}).

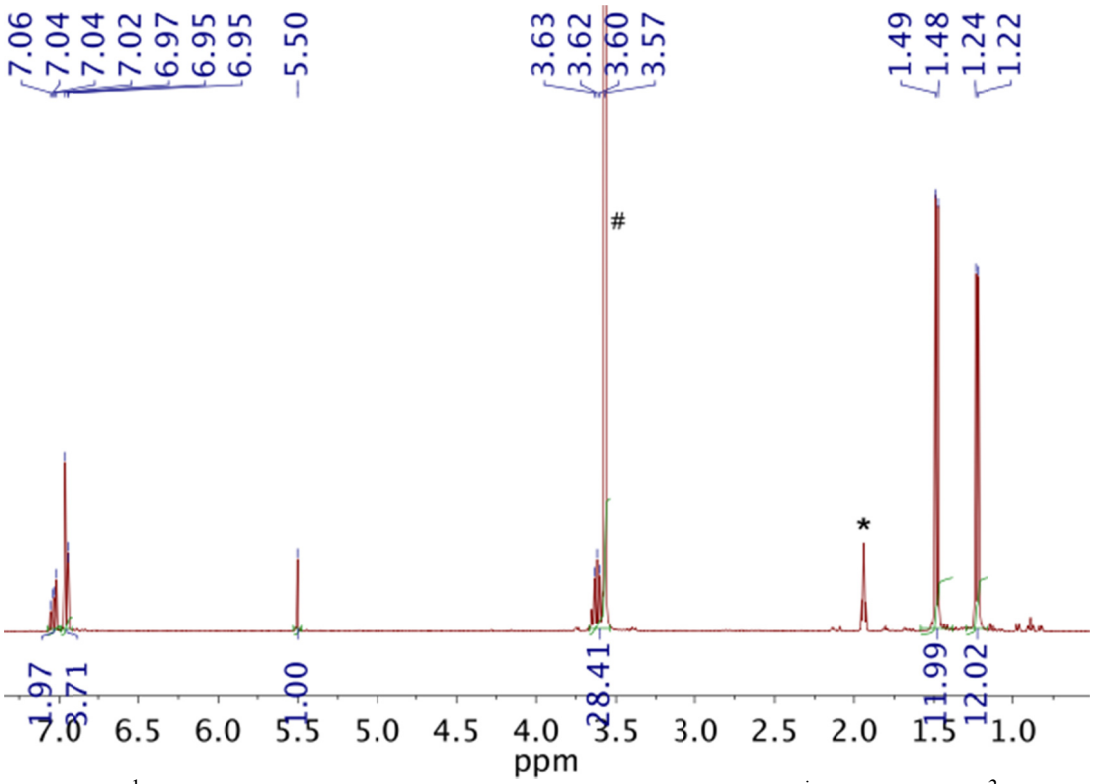

Figure S12. ^{1}H NMR spectrum (399 MHz, 298 K, CD$_3$CN) of [^{i}Pr$_2$NN$_{F6}$]Ni(κ^2-O$_2$N$_2$)K[18-crown-6] (**3a**). The resonances marked with (*) and (#) are from the solvent residual peak for acetonitrile-d_3 and 18-crown-6, respectively.

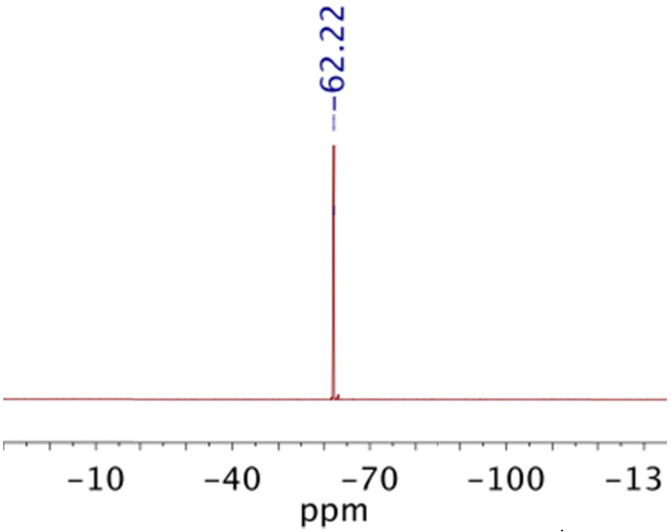

Figure S13. ^{19}F NMR spectrum (376 MHz, 298 K, CD_3CN) of [$^{i}Pr_2NN_{F6}$]Ni(κ^2-O_2N_2)K[18-crown-6] (**3a**).

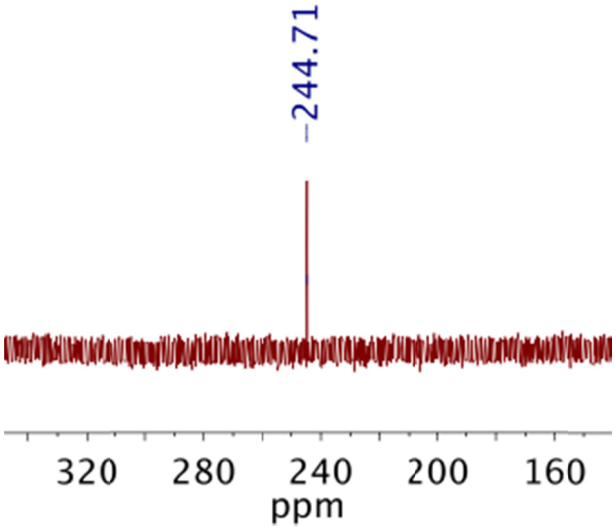

Figure S14. ^{15}N NMR spectrum (41 MHz, 298 K, CD_3CN) of [$^{i}Pr_2NN_{F6}$]Ni(κ^2-$O_2{}^{15}N_2$)K[18-crown-6] (**3a**-$^{15}N^{15}N$).

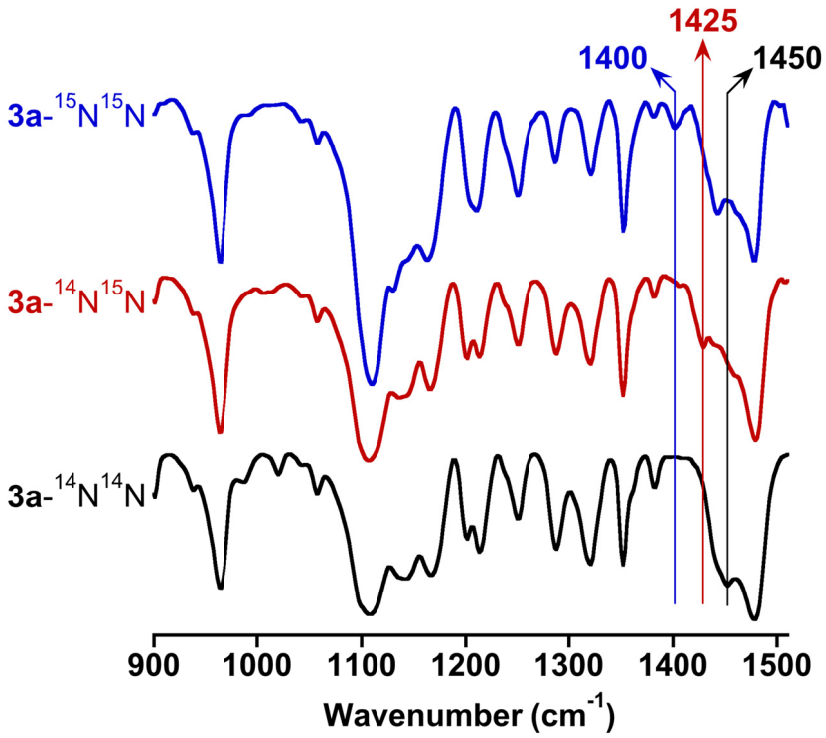

Figure S15. FT-IR (KBr pellet) spectra of **3a**-$^{14}N^{14}N$ (black trace), **3a**-$^{14}N^{15}N$ (red trace), and **3a**-$^{15}N^{15}N$ (blue trace). The ν(N=N) at 1450 cm^{-1} (for **3a**-$^{14}N^{14}N$, black trace) downshifts to 1425 cm^{-1} (red trace) and 1400 cm^{-1} (blue trace) for a mixed labeled sample **3a**-$^{14}N^{15}N$ and completely labeled sample **3a**-$^{15}N^{15}N$, respectively. Notably, the observed $^{15}N/^{14}N$-shifts $^{15N/14N}\Delta\nu$ (N=N) follow predicted shifts by Hooke's Law.

7. Synthesis and Characterization of [^{i}Pr$_2$NN$_{F6}$]Ni(κ^2-O$_2$N$_2$)K[2.2.2-cryptand] (3b).

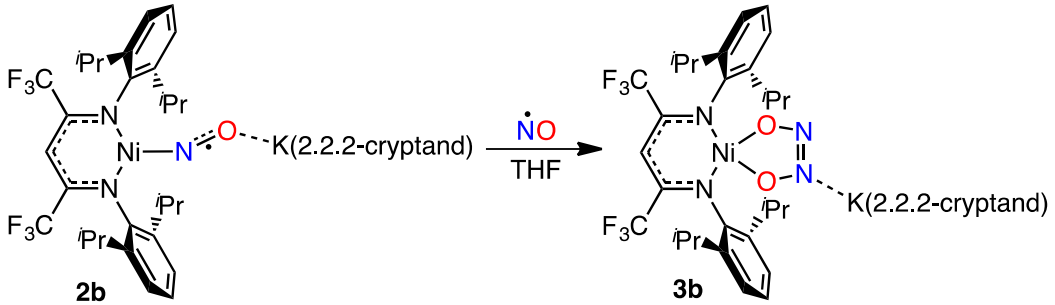

Scheme S5. Synthesis of [^{i}Pr$_2$NN$_{F6}$]Ni(κ^2-O$_2$N$_2$)K[2.2.2-cryptand] (**3b**).

A solution of [^{i}Pr$_2$NN$_{F6}$]Ni(μ-η^2:η^2-NO)K[2.2.2-cryptand] (**2b**) (0.420 g, 0.408 mmol) in tetrahydrofuran (*ca.* 10 mL) was placed into a Schlenk tube capped with a septum. At room temperature, NO$_{(g)}$ (1 equiv.: 10.0 mL, 1.0 atm, 0.409 mmol) was slowly injected to the solution of **2b** and the color of the solution immediately changed from dark brownish purple to brownish red. After stirring 15 min, the resultant solution was evaporated to dryness and the crude product was obtained as brown powder. The crude material was thoroughly washed with pentane (*ca.* 20 mL) and dried to afford a brownish solid **3b** (0.385 g, 0.363 mmol) in 89% yield. Slow evaporation of solvent from a concentrated tetrahydrofuran solution of **3b** at room temperature resulted in X-ray quality crystals. Anal. Calcd for $C_{47}H_{71}F_6N_6O_8NiK$: C, 53.26; H, 6.75; N, 7.93. Found: C, 53.01; H, 7.05; N, 7.66. ^{1}H NMR (400 MHz, CD_3CN): δ 7.04 (t, 2H, *p*-Ar-*H*), 6.96 (d, 4H, *m*-Ar-*H*), 5.50 (s, 1H, backbone-C*H*), 3.62 (hept, 4H, -C*H*Me$_2$), 3.56 (s, 12H, -C*H*$_2$- from cryptand), 3.51 (t, 12H, -C*H*$_2$- from cryptand), 2.52 (t, 12H, -C*H*$_2$- from cryptand), 1.49 (d, 12H, -CH*Me*$_2$), 1.23 (d, 12H, -CH*Me*$_2$). ^{13}C{^{1}H} NMR (100 MHz, CD_3CN): δ 148.23 (q, $^2J_{CF}$ = 25.5 Hz), 144.49, 143.27, 129.30, 126.02, 122.91, 120.68 (q, $^1J_{CF}$ = 284.3 Hz), 87.72 (p, $^3J_{CF}$ = 5.8 Hz), 71.24, 68.46, 54.73, 29.63, 25.37, 23.32. ^{19}F NMR (376 MHz, CD_3CN): δ -62.22.

^{15}N-labelled [^{i}Pr$_2$NN$_{F6}$]Ni(κ^2-O$_2$^{15}N$_2$)K[2.2.2-cryptand] (**3b-**^{15}N^{15}N) was prepared from **2b-**^{15}N by addition of 1 equiv. ^{15}NO from a labelled nitric oxide cylinder that was handled inside the glovebox without further purification due to the small amount employed and high cost of ^{15}NO.

8. Synthesis and Characterization of $\{[^{i}Pr_2NN_{F6}]Ni\}_2(\mu\text{-}OH)_2$ (4).

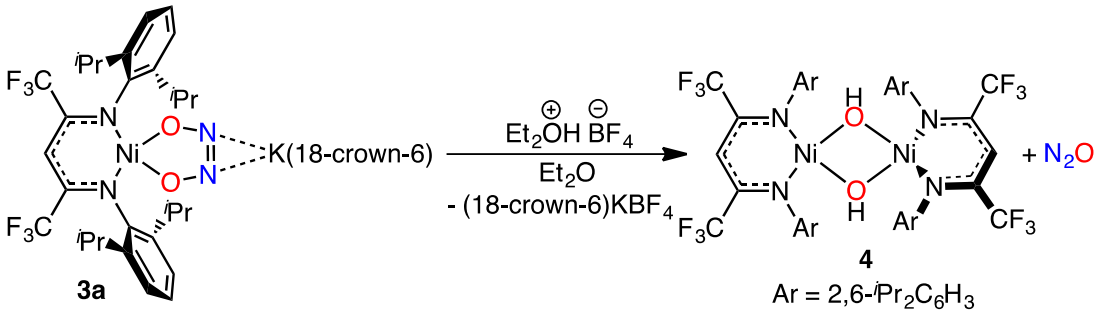

Scheme S6. Synthesis of $\{[^{i}Pr_2NN_{F6}]Ni\}_2(\mu\text{-}OH)_2$ (**4**) from $[^{i}Pr_2NN_{F6}]Ni(\kappa^2\text{-}O_2N_2)K$[18-crown-6] (**3a**).

Tetrafluoroboric acid diethyl ether complex (0.061 g, 52.0 µL, 0.382 mmol) was added to a vigorously stirring solution of $[^{i}Pr_2NN_{F6}]Ni(\kappa^2\text{-}O_2N_2)K$[18-crown-6] (**3a**) (0.389 g, 0.382 mmol) in ditheyl ether. The color of the resultant reaction mixture immediately changed from brownish to orange with concomitant evolution of gas. After *ca.* 5 min of stirring, the reaction mixture was filtered and the filtrate was evaporated to dryness to afford a brownish powder **4** (151.9 g, 0.126 mmol) in 66% yield. X-ray quality crystals were grown from a concentrated solution of **4** in diethyl ether and pentane (1:1) at -40 °C. Anal. Calcd for $C_{58}H_{72}F_{12}N_4O_2Ni_2$: C, 57.93; H, 6.03; N, 4.66. Found: C, 57.66; H, 6.39; N, 4.64.

Coformation of N_2O was confirmed by solution IR and ^{15}N NMR spectroscopy (See Section 9). Both solution IR and ^{15}N NMR spectroscopic studies (Section 9) indicate smooth conversion of hyponitrite to N_2O.

9. Detection of N_2O upon Protonation of [$^{i}Pr_2NN_{F6}$]Ni(κ^2-O_2N_2)K[18-crown-6] (3a).

Detection of NO upon Acidification with Trifluoroacetic Acid. [$^{i}Pr_2NN_{F6}$]Ni(κ^2-O_2N_2)K[18-crown-6] (**3a**) (0.117 g, 0.114 mmol) was dissolved in 3.0 mL tetrahydrofuran and the solution was placed into a 3-neck Schlenk tube capped with septa. An optical probe (ReactIR) was inserted into the solution for monitoring the reaction by solution IR spectroscopy. Then one equivalent trifluoroacetic acid (8.7 μL, 0.114 mmol) was injected into the solution and the color of the reaction mixture immediately changed. A new vibrational band at 2227 cm^{-1} (for the generation N_2O) immediately developed with simultaneous decay of a feature at 1475 cm^{-1} (for the consumption of **3a**).

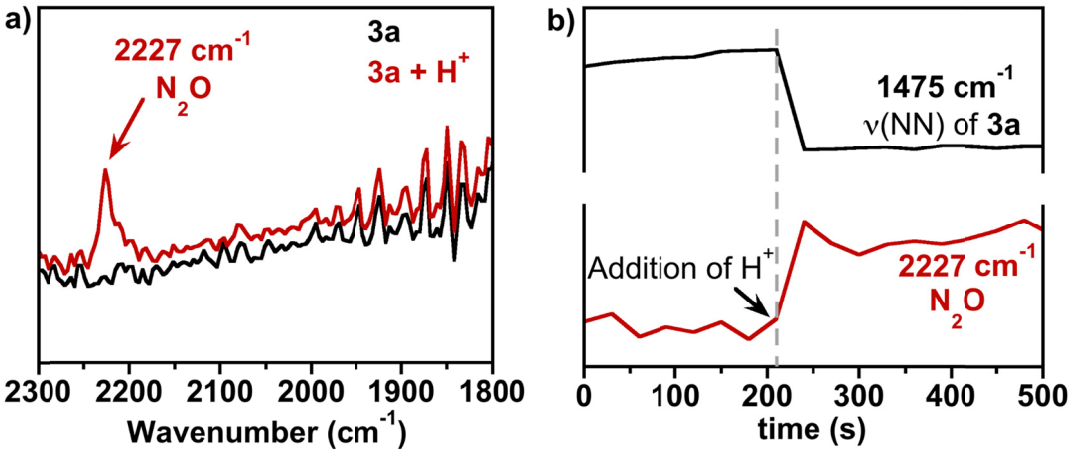

Figure S16. (a) Infrared spectra of a tetrahydrofuran solution (38.0 mM) of [$^{i}Pr_2NN_{F6}$]Ni(κ^2-O_2N_2)K[18-crown-6] (**3a**) before (black trace) and after (red trace) addition of one equivalent trifluoroacetic acid at room temperature. The vibrational feature at 2227 cm^{-1} arises due to the generation of N_2O. (b) Time traces obtained from solution infrared spectroscopy demonstrates the generation of N_2O from [$^{i}Pr_2NN_{F6}$]Ni(κ^2-O_2N_2)K[18-crown-6] (**3a**) upon protonation.

Quantification of N_2O upon Protonation with HBF_4•OEt_2. Gas chromatography was performed on a Gow-Mac GC (Model 69-400 TCD) equipped with a TCD as well as a 6' × 1/8" Molesieve 13x column. The carrier gas was He, and throughout the entire separation, the column was kept at 60 °C, while the detector was at 100 °C. Using identical reaction vessels and solvent amounts, the identification and quantification of N_2O was accomplished by withdrawing 250 μL of the headspace using a 250 μL Hamilton 1725 sample lock gastight syringe equipped with a large removable needle (22s ga, 2 in, point style 2).

A calibration curve was generated by preparing vials containing known amounts of pure N_2O gas for reference. This was accomplished by injecting varying amounts of N_2O in a stirring solution of diethyl ether (3 mL) and HBF_4•Et_2O (7.24 µL), contained in 20 mL glass-vials, capped with rubber septum and sealed with parafilm. Quantification of N_2O was accomplished by withdrawing 250 µL of the headspace using a gastight syringe and injecting into the GC. The calibration curve was generated by plotting the area of N_2O (as obtained from the gas chromatograms) *vs* volume of added N_2O (in mL).

Calibration curve used for the quantification of N_2O

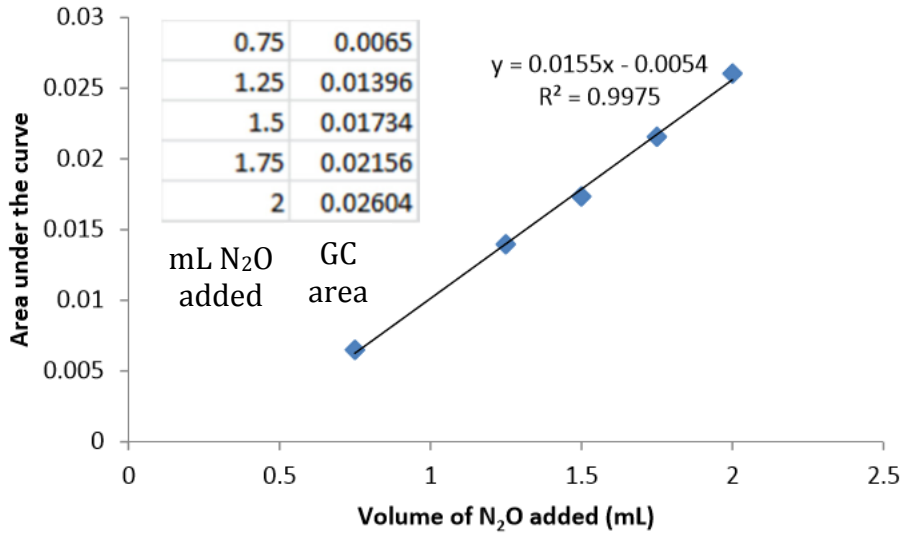

Release of N_2O upon Acidification of 3a with HBF_4•OEt_2. Inside a nitrogen filled glovebox, [^{i}Pr$_2$NN$_{F6}$]Ni(κ^2-O_2N_2)K[18-crown-6] (**3a**) (0.050 g, 0.053 mmol) was added into a 20 mL glass vial and was dissolved in diethyl ether (3 mL). The vial was capped with a rubber septum and was sealed with parafilm. HBF_4•OEt_2 (7.24 µL, 0.053 mmol) was injected using a micro-syringe and the solution was vigorously stirred for 5 min. The color of the solution changed from light brown to yellowish-orange. Quantification of N_2O produced from the reaction was accomplished by withdrawing 250 µL of the headspace and injecting the same in GC. Based on the theoretical volume of N_2O that should be formed (100 % conversion = 0.053 mmol × 24.45 mL/mmol = 1.29 mL (at 1 atm, 298 K)), the volume of N_2O detected from experiment (0.98 mL) corresponded to a 76 % yield of N_2O.

Observation of N_2O by ^{15}N NMR upon Protonation with Trifluoroacetic Acid. ^{15}N enriched sample of [$^{i}Pr_2NN_{F6}$]Ni(κ^2-$O_2{}^{15}N_2$)K[18-crown-6] (**3a**-$^{15}N^{15}N$) (0.042 g, 0.041 mmol) was dissolved in *ca.* 0.6 mL tetrahydrofuran-d_8 and the solution was placed in an NMR tube capped with a septum. Then 1 equiv. trifluoroacetic acid (3.5 µL, 0.041 mmol) was injected into the solution and the resultant reaction mixture was analyzed by ^{15}N NMR (41 MHz, 25 °C).

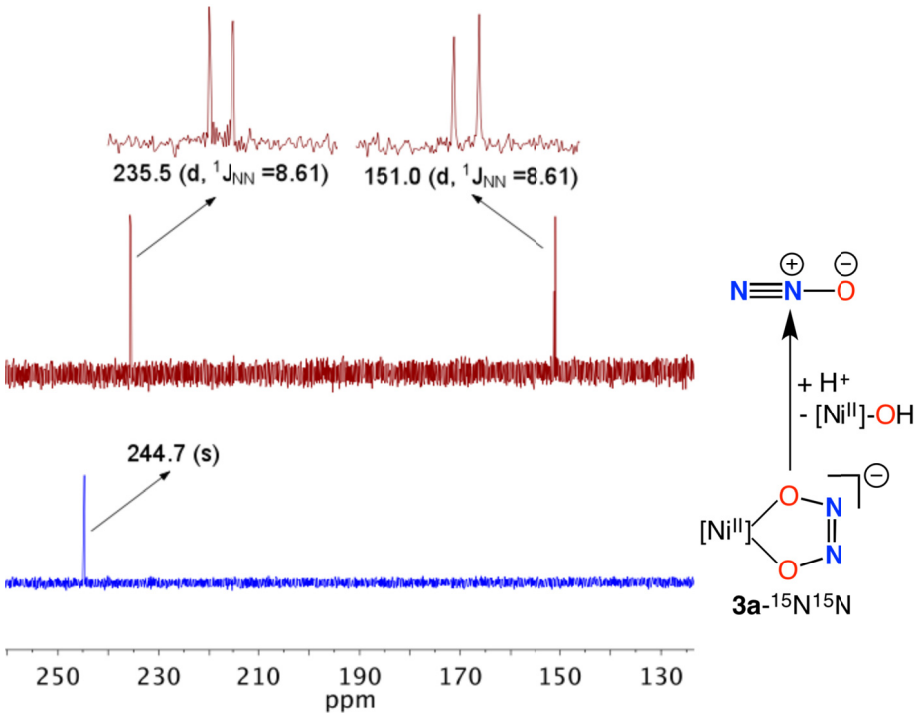

Figure S17. Comparison of ^{15}N NMR spectra (41 MHz, 298 K, tetrahydrofuran-d_8) of [$^{i}Pr_2NN_{F6}$]Ni(κ^2-$O_2{}^{15}N_2$)K[18-crown-6] (**3a**-$^{15}N^{15}N$) (blue trace) and the crude reaction mixture (red trace) obtained upon addition of one equivalent trifluoroacetic acid to a solution of **3a**-$^{15}N^{15}N$ in tetrahydrofuran-d_8. Insets highlight two doublets at δ = 235.5 (d, $^1J_{NN}$ = 8.61 Hz) and 151.0 (d, $^1J_{NN}$ = 8.61 Hz) that appear from the two chemically inequivalent nitrogen atoms in $^{15}N_2O$.[4]

10. X-Band EPR Spectra of 2a and 2b.

General considerations. EPR spectra were collected on a JEOL continuous wave spectrometer JES-FA200 equipped with an X-band Gunn oscillator bridge, a cylindrical mode cavity, and a liquid nitrogen cryostat. EPR measurements were performed in sealed quartz tubes. All spectra were obtained on freshly prepared solutions in THF of at least two independently synthesized batches and were checked carefully for reproducibility. Background spectra were obtained on clean solvents at the same measurement conditions.

Spectral simulation of room temperature spectra was performed using the program QCMP 136 by Prof. Dr. Frank Neese from the Quantum Chemistry Program Exchange as used by Neese *et al*.[5] The fittings were performed by the "chi by eye" approach and always taking all available spectra at different temperatures into account. Collinear *g* and *A* tensors were used.

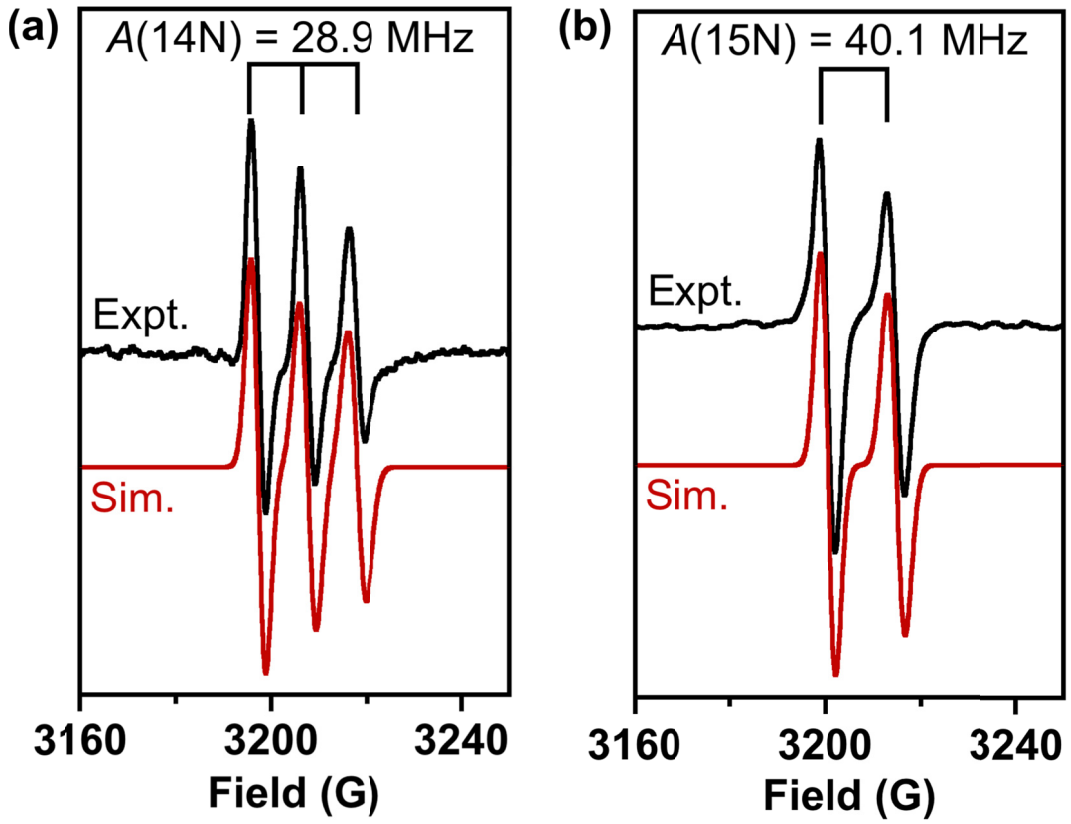

Figure S18. Isotropic X-band EPR spectra (black trace) and simulation (red trace) of [^{i}Pr$_2$NN$_{F6}$]Ni(μ-η^2:η^2-NO)K[18-crown-6](THF) (**2a**) (Figure S18a) and [^{i}Pr$_2$NN$_{F6}$]Ni(μ-η^2:η^2-^{15}NO)K[18-crown-6](THF) (**2a**-^{15}N) (Figure S18b) in tetrahydrofuran at 293 K. Frequency = 8.982883 GHz, power = 0.99 mW, ModWidth = 0.35 mT, time-constant = 0.03 s. Simulation provides g_{iso} = 2.0008, A_{iso}(^{14}N) = 28.9 MHz (for **2a**), and A_{iso}(^{15}N) = 40.1 MHz (for **2a**-^{15}N), W_{iso} = 2.05 mT. As expected, the ratio of isotropic ^{15}N and ^{14}N hyperfine coupling constants A(^{15}N)/A(^{14}N) = 1.39 is very close to the ratio of their gyromagnetic ratios γ(^{15}N)/γ(^{14}N) =1.40.

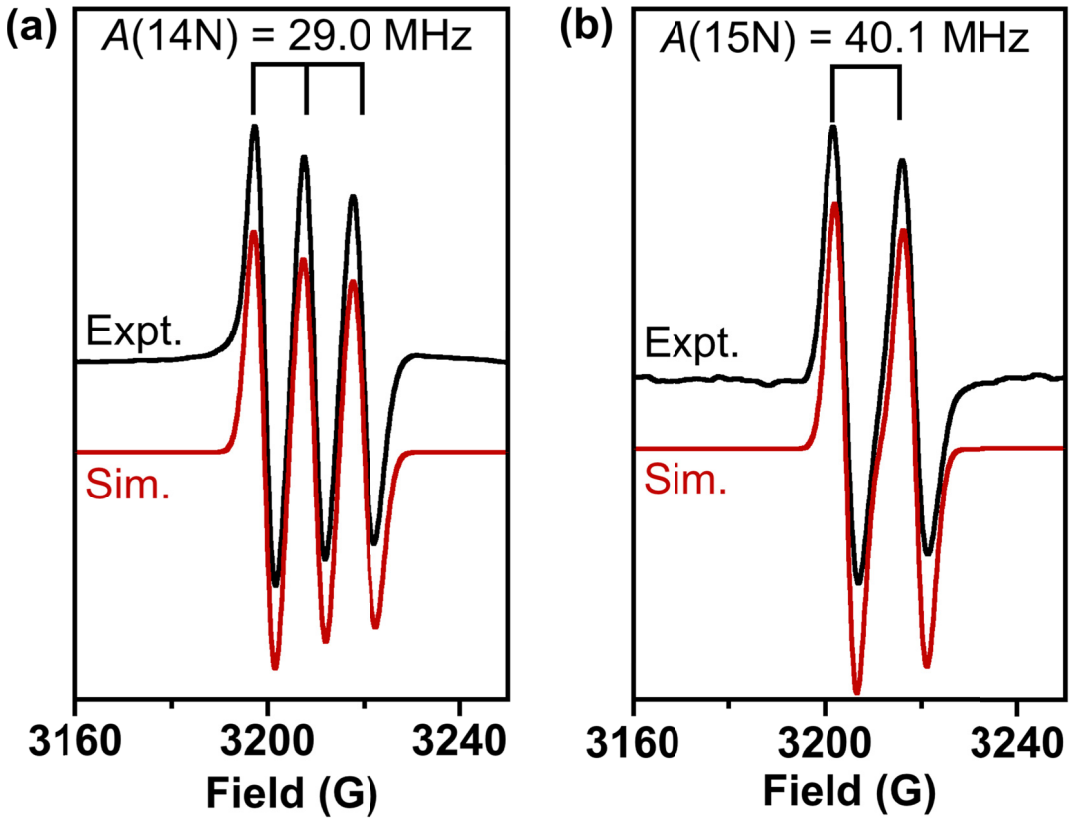

Figure S19. Isotropic X-band EPR spectrum (black trace) and simulation (red trace) of [^{i}Pr$_2$NN$_{F6}$]Ni(μ-η^1:η^1-NO)K[2.2.2-cryptand] (**2b**-^{14}N) (Figure S19a) and [^{i}Pr$_2$NN$_{F6}$]Ni(μ-η^1:η^1-^{15}NO)K[2.2.2-cryptand] (**2b**-^{15}N) (Figure S19b) in tetrahydrofuran at 293 K. Frequency = 8.973624 GHz, power = 0.99 mW, ModWidth = 0.35 mT, time-constant = 0.03 s. Simulation provides g_{iso} = 1.99740, A_{iso}(^{14}N) = 29.0 MHz (for **2b**), and A_{iso}(^{15}N) = 40.1 MHz (for **2b**-^{15}N), W_{iso} = 2.8 mT. As expected, the ratio of isotropic ^{15}N and ^{14}N hyperfine coupling constants A(^{15}N)/A(^{14}N) = 1.38 is very close to the ratio of their gyromagnetic ratios γ(^{15}N)/γ(^{14}N) =1.40.

Low Temperature EPR fit details. Low temperature EPR data for [^{i}Pr$_2$NN$_{F6}$]Ni(μ-η^2:η^2-NO)K[18-crown-6](THF) (**2a**), [^{i}Pr$_2$NN$_{F6}$]Ni(μ-η^2:η^2-^{15}NO)K[18-crown-6](THF) (**2a**-^{15}N), and [^{i}Pr$_2$NN$_{F6}$]Ni(μ-η^1:η^1-NO)K[2.2.2-cryptand] (**2b**) were modeled using Easyspin[a] for MATLAB® and guided by DFT calculations (see computational section). Starting parameters for g_x, g_y, g_z and $A_{x,y,z}$(^{14}NO), $A_{x,y,z}$(^{i}Pr$_2$^{14}NNF$_6$), and $A_{x,y,z}$(^{i}Pr$_2$N^{14}NF$_6$) were taken directly from DFT calculations for linear and side-on species and Nelder/Mead simplex fits of the integrated data were conducted in Easyspin. While slight g-anisotropy was predicted for **2a** by DFT calculations, a satisfactory fit could not be achieved. The best model for the experimental data utilized an isotropic g for **2a**, but included the wider g anisotropy predicted for end-on **2b**. The starting parameters for the ^{15}N data were taken to be the best fit parameters from the ^{14}N data and all the A_{NO} values were multiplied by the gyromagnetic ratio γ(^{15}N)/γ(^{14}N) =1.38, in agreement with the room temperature data.

Computational details. EPR calculations were conducted with the CP(PPP) basis set on nickel,[b] the IGLO-III basis set on nitrogen and oxygen,[c] and the TZVP basis set on all other atoms.[d] A dense integration grid with an integration accuracy of 11 on Ni and 9 on N, O, and K was applied to increase radial integration accuracy. All calculations were examined to ensure that the electronic structural description did not significantly alter.

Table S1. Collection of parameters used to fit low T EPR spectra of **2a** and **2a**-^{15}N.

		2a (side-on)			**2b (end-on)**		
		Exp. Fit		**Calc.**	**Exp. Fit**		**Calc.**
		^{14}N	**^{15}N**	**^{14}N**	**^{14}N**	**^{15}N**	**^{14}N**
Weight		38%			62%		
Linewidth		2.0	2.5		1.8	1.8	
g	g_1	2.005	2.005	1.943	1.912	1.912	1.999
	g_2	2.005	2.005	1.980	1.974	1.974	2.082
	g_3	2.005	2.005	2.004	2.022	2.022	2.165
	g_{iso}	2.005	2.005	1.976	1.969	1.969	2.082
N^{a}O	A_1	12.00	16.56	9.080	10.00	13.8	2.428
	A_2	-10.00	-13.80	-20.176	-40.00	-55.20	-54.175
	A_3	101.00	140.00	89.185	50.72	96.60	88.716
	A_{iso}			26.029			12.323
^{i}Pr$_2$N^{b}NF$_6$	A_1	-4.95	-4.95	-4.948	12.01	12.01	12.011
	A_2	-5.55	-5.55	-5.555	14.02	14.02	14.025
	A_3	-6.14	-6.14	-6.141	16.65	16.65	16.524
	A_{iso}			-5.548			14.187
^{i}Pr$_2$NN^{c}F$_6$	A_1	-2.02	-2.02	-2.023	7.04	7.04	7.046
	A_2	-2.61	-2.61	-2.609	7.55	7.55	7.550
	A_3	-3.59	-3.59	-3.595	10.31	10.31	10.311
	A_{iso}			-2.742			8.303

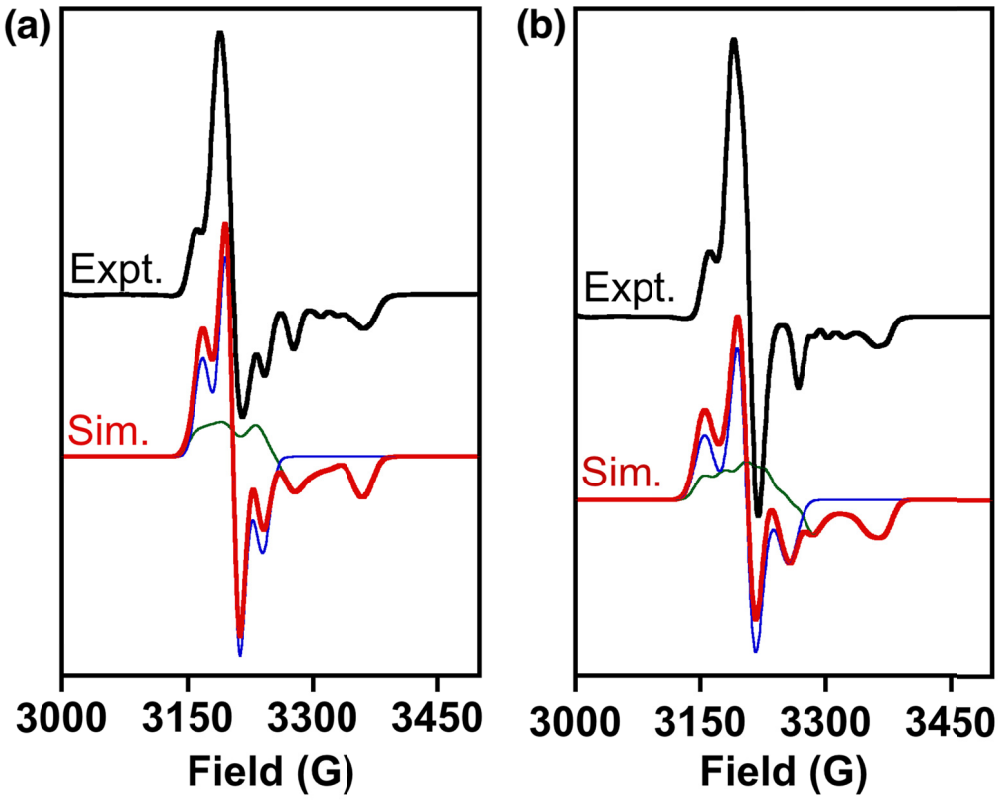

Figure S20. Frozen glass X-band EPR spectrum (black trace) and simulation (red trace) of [^{i}Pr$_2$NN$_{F6}$]Ni(μ-η^2:η^2-NO)K[18-crown-6](THF) (**2a**) (Figure S20a) and [^{i}Pr$_2$NN$_{F6}$]Ni(μ-η^2:η^2-^{15}NO)K[18-crown-6](THF) (**2a**-^{15}N) (Figure S20b) in tetrahydrofuran at 20 K. Frequency = 8.99 GHz, power = 0.99 mW, ModWidth = 1.0 mT, time-constant = 0.01 s. Simulated spectrum (red trace) is modeled by employing a combination of blue trace (38%, from side-on) and green trace (62%, from end-on). For the side-on species (blue trace), simulation employed $g_1 = g_2 = g_3 = 2.005$ with $A_1(^{14}N_{NO}) = 12.00$ MHz, $A_2(^{14}N_{NO}) = -10.00$, $A_3(^{14}N_{NO}) = 101.00$ MHz (for **2a**) and $A_1(^{15}N_{NO}) = 16.56$ MHz, $A_2(^{15}N_{NO}) = -13.80$, $A_3(^{15}N_{NO}) = 140.00$ MHz (for **2a**-^{15}N). For end-on species (green trace), simulation provides $g_1 = 2.022$, $g_2 = 1.974$, $g_3 = 1.912$ with $A_1(^{14}N_{NO}) = 21.73$ MHz, $A_2(^{14}N_{NO}) = -40.00$, $A_3(^{14}N_{NO}) = 50.72$ MHz (for **2a**) and $A_1(^{15}N_{NO}) = 30.00$ MHz, $A_2(^{15}N_{NO}) = -55.20$, $A_3(^{15}N_{NO}) = 70.00$ MHz (for **2a**-^{15}N). Additional hyperfine coupling to the N-atoms of the ^{i}Pr$_2$NNF$_6$ ligand was included (see Table S1).

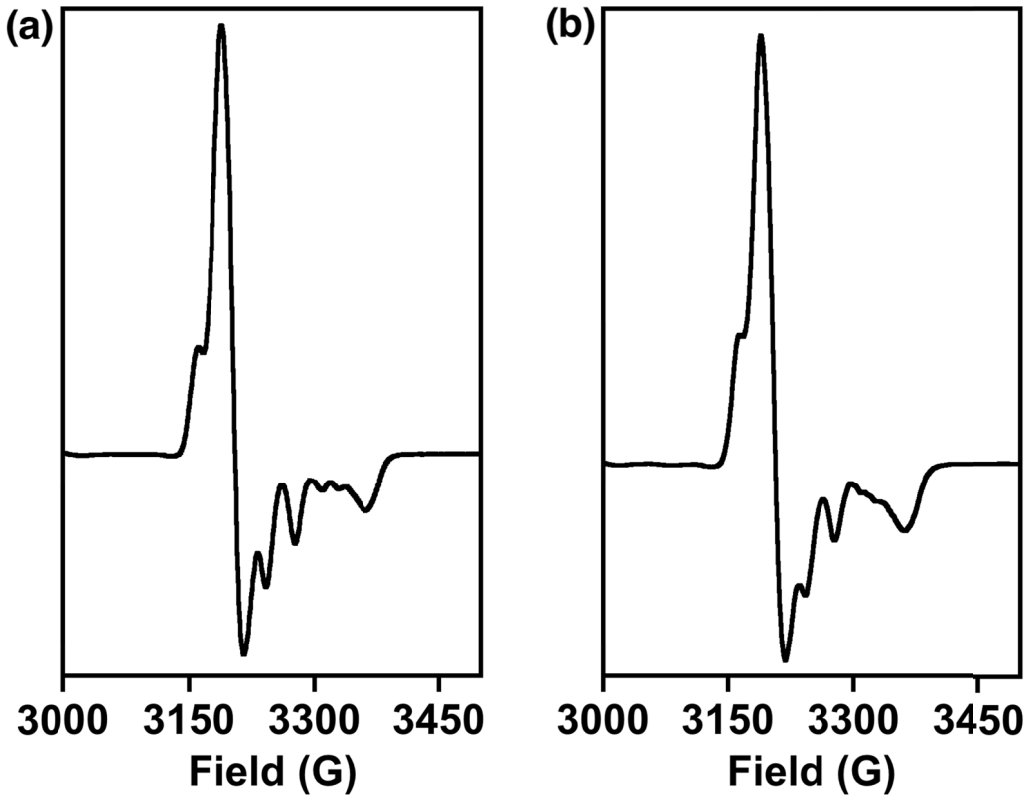

Figure S21. Frozen glass X-band EPR spectra of [^{i}Pr$_2$NN$_{F6}$]Ni(μ-η^2:η^2-NO)K[18-crown-6](THF) (**2a**) (Figure S21a) and [^{i}Pr$_2$NN$_{F6}$]Ni(μ-η^1:η^1-NO)K[2.2.2-cryptand] (**2b**) (Figure 21b) in tetrahydrofuran at 20 K. Frequency = 8.99 GHz, power = 0.99 mW, ModWidth = 0.5 mT, time-constant = 0.01 s.

References for Calculation and Simulation of EPR Parameters

(a) Stoll, S.; Schweiger, A. *J. Magn. Reson.* **2006**, *178*, 42.
(b) Kirchner, B.; Wennmohs, F.; Yes, S.; Neese, F. *Curr. Opin. Chem. Biol.* **2007**, *11*, 134.
(c) Kutzelnigg, W.; Fleischer, U.; Chindler, M. The IGLO-Method: Ab Initio Calculation and Interpretation of NMR Chemical Shifts and Magnetic Susceptibilities; Springer Verlag: Heidelberg, **1990**; Vol. 23.
(d) Schaefer, A.; Horn, H.; Ahlrichs, R. *J. Chem. Phys.* **1992**, *97*, 2571.

11. Crystallographic Details.

Single crystals of each compound [^{i}Pr$_2$NN$_{F6}$]NiNO (**1**) (CCDC 1565623), [^{i}Pr$_2$NN$_{F6}$]Ni(μ-η^2:η^2-NO)K[18-crown-6](THF) (**2a**) (CCDC 1565624), [^{i}Pr$_2$NN$_{F6}$]Ni(μ-η^1:η^1-NO)K[2.2.2-cryptand] (**2b**) (CCDC 1565625), [^{i}Pr$_2$NN$_{F6}$]Ni(κ^2-O$_2$N$_2$)K[18-crown-6] (**3a**) (CCDC 1565626), [^{i}Pr$_2$NN$_{F6}$]Ni(κ^2-O$_2$N$_2$)K[2.2.2-cryptand] (**3b**) (CCDC 1565627), and {[^{i}Pr$_2$NN$_{F6}$]Ni}$_2$(μ-OH)$_2$ (**4**) (CCDC 1565628) were mounted under mineral oil on glass fibers and immediately placed in a cold nitrogen stream at 100(2) K prior to data collection. Data for compounds **3a** and **3b** were collected on a Bruker D8 Quest equipped with a Photon100 CMOS detector and a MoImS source. Data for compounds **1**, **2a**, **2b**, and **4** were collected on a Bruker DUO equipped with an APEXII CCD detector and Mo fine focus sealed tube source. Either full spheres (triclinic) or hemispheres (monoclinic or higher) of data were collected (0.3° or 0.5°ω-scans; $2\theta_{max}$ = 56°; monochromatic Mo Kα radiation, λ = 0.7107 Å) depending on the crystal system and integrated with the Bruker SAINT program. Structure solutions were performed using the SHELXTL/PC suite[6,7] and XSEED.[8] Intensities were corrected for Lorentz and polarization effects and an empirical absorption correction was applied using Blessing's method as incorporated into the program SADABS.[9] Non-hydrogen atoms were refined with anisotropic thermal parameters and hydrogen atoms were included in idealized positions. Structures were rendered with POV-Ray in XSEED using 50% probability ellipsoids. Further comments on disorder models:

[^{i}Pr$_2$NN$_{F6}$]Ni(μ-η^2:η^2-NO)K[18-crown-6](THF) (2a).

There are two symmetrically independent molecules in the asymmetric unit. One isopropyl group on molecule one is disordered over two positions. The like C-C distances were restrained to be similar. The THF molecule coordinated to K1 is disordered over two positions. The K-O, O-C, and C-C distances were restrained to be similar. On molecule two, the crown ether is disordered over two positions. The like K-O, O-C, and C-C distances were restrained to be similar. The THF molecule coordinated to K2 is also disordered over two positions. The like K-O, O-C, and C-C distances were restrained to be similar. Similar displacement amplitudes were imposed on disordered sites overlapping by less than the sum of van der Waals radii. The relative identities of the N/O atoms of the nitrosyl group were established via testing several models in which the N and O atoms were switched. While

there was not a large difference in models that have inverted N and O positions, ultimately the orientation that produced the best displacement parameters as well as the lowest R1/wR2 values was selected. This model is discussed in the manuscript and appears in Figures 2, S23a, and S23b.

Modeling of N/O positional disorder. Starting from the refinement above, we examined N/O positional disorder by assigning each independent molecule of **2a** two sets of N and O atoms in which the respective N and O positions are inverted (N/O and O/N). While the positions of each set of N and O atoms were allowed to refine, the N-O distances were restrained to be similar. Similar displacement amplitudes were imposed on disordered sites overlapping by less than the sum of van der Waals radii. Two orientations in each independent molecule refine to 56:44 (molecule 1) and 53:47 (molecule 2). Unfortunately, the uncertainties in the N and O positions are much higher those in the initial model that leads to much greater uncertainties in the N-O distances (molecule 1: 1.28(10), 1.32(7) Å; molecule 2: 1.306(18), and 1.302(18) Å) than in the original refinement (1.270(6) Å; molecule 2: 1.284(6) Å) along with a much wider range of Ni-N and Ni-O distances. These appear in Figures S23c and S23d.

[^{i}Pr$_2$NN$_{F6}$]Ni(μ-η^1:η^1-NO)K[2.2.2-cryptand] (2b).

A structural model consisting of the host plus three highly disordered fluorobenzene solvate molecules per asymmetric unit was developed; however, positions for the idealized solvate molecules were poorly determined. This model converged with wR2 = 0.2701 and R1 = 0.0805 for 1033 parameters with 1371 restraints against 12678 data. Since positions for the solvate molecules were poorly determined a second structural model was refined with contributions from the solvate molecules removed from the diffraction data using the bypass procedure in PLATON. No positions for the host differed by more than two su's between these two refined models. The electron count from the "squeeze" model converged in good agreement with the number of solvate molecules predicted by the complete refinement.

The NO group is disordered over three positions. The primary orientation (77%) is end-on while the two minor (16% and 7%) orientations are both side-on. For the two side-on orientations that feature inverted N/O position, the Ni-N and Ni-O distances were restrained to be similar. Both CF_3 groups are disordered over two positions. The like C-C, C-F, and F-F distances were restrained to be. One C_2H_4 group of the kryptofix ligand is disordered over

two positions. The like C-C and C-O distances were restrained to be similar. Similar displacement amplitudes were imposed on disordered sites overlapping by less than the sum of van der Waals radii.

[^{i}Pr$_2$NN$_{F6}$]Ni(κ^2-O$_2$N$_2$)K[18-crown-6] (3a).

A structural model consisting of the host plus a highly disordered partial occupancy diethyl ether solvate molecule was developed; however, positions for the idealized solvate molecules were poorly determined. This model converged with wR2 = 0.0898 and R1 = 0.0349 for 810 parameters with 582 restraints against 9019 data. Since positions for the solvate molecule were poorly determined a second structural model was refined with contributions from the solvate molecule removed from the diffraction data using the bypass procedure in PLATON. No positions for the host differed by more than two su's between these two refined models. The electron count from the "squeeze" model converged in good agreement with the number of solvate molecules predicted by the complete refinement.

One CF_3 group is disordered over two positions. The like C-C, C-F, and F-F distances were restrained to be similar. Two of the isopropyl groups are disordered over two positions. The like C-C distances were restrained to be similar. A portion of the crown ether is disordered over two positions. The like C-C, O-C, and O-K distances were restrained to be similar. Similar displacement amplitudes were imposed on disordered sites overlapping by less than the sum of van der Waals radii.

{[^{i}Pr$_2$NN$_{F6}$]Ni}$_2$(μ-OH)$_2$ (4).

The two bridging hydroxides are disordered over two sites. The like Ni-O distances were restrained to be similar. One of the CF_3 groups is disordered over three positions. The like C-C, C-F, and F-F distances were restrained to be similar. Two other CF_3 groups are disordered over two positions. The like C-C, C-F, and F-F distances were restrained to be similar. Two isopropyl groups are disordered over two sites. The like C-C distances were restrained to be similar. The two methyl groups of another isopropyl are disordered over two sites. The like C-C distances were restrained to be similar. Similar displacement amplitudes were imposed on disordered sites overlapping by less than the sum of van der Waals radii.

The hydroxyl H atoms on the major component of disordered sites were located in the difference map and their positions were allowed to refine. The O-H distance was

restrained to be 0.84Å. The H atoms for the minor component of the disordered hydroxyls could not be located in the difference map, and thus were not added to the model.

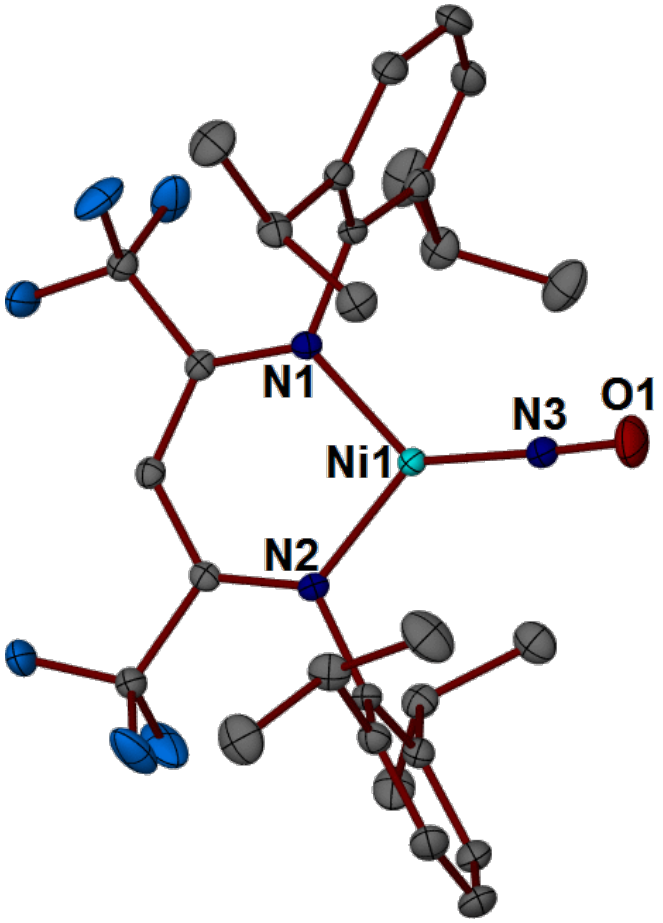

Figure S22. Molecular structure of [^{i}Pr$_2$NN$_{F6}$]NiNO (**1**) (CCDC 1565623). The thermal ellipsoid plots are drawn at 50% probability level. Hydrogen atoms are omitted for clarity. Selected bond distances (Å) and angles (°): Ni1-N1 1.8899(10), Ni1-N2 1.8887(10), Ni1-N3 1.6280(11), N3-O1 1.1602(15), N1-Ni1-N2 97.29(4), N1-Ni1-N3 129.76(5), N2-Ni1-N3 132.77(5), Ni1-N3-O1 174.47(11).

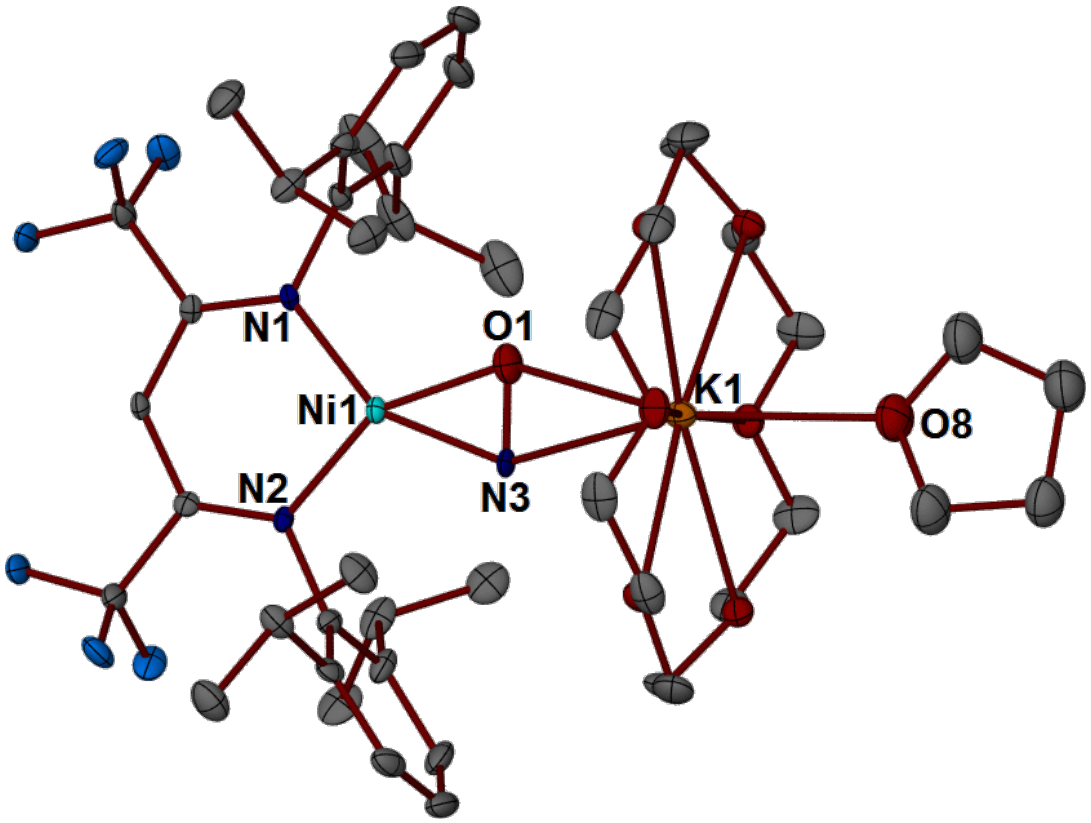

Figure S23a. X-ray structure of one of the two unique molecules of [^{i}Pr$_2$NN$_{F6}$]Ni(μ-η^2:η^2-NO)K[18-crown-6](THF) (**2a**) (CCDC 1565624) in the unit cell. The thermal ellipsoid plots are drawn at 30% probability level. Hydrogen atoms are omitted for clarity. Selected bond distances (Å) and angles (°) for molecule 1: Ni1-N1 1.866(4), Ni1-N2 1.863(4), Ni1-N3 1.853(5), Ni1-O1 1.839(5), N3-O1 1.270(6), Ni1•••K1 4.417, N1-Ni1-N2 99.63(18), N1-Ni1-O1 110.2(2), N2-Ni1-N3 109.9(2), O1-Ni1-N3 40.2(2), Ni1-N3-O1 69.3(3).

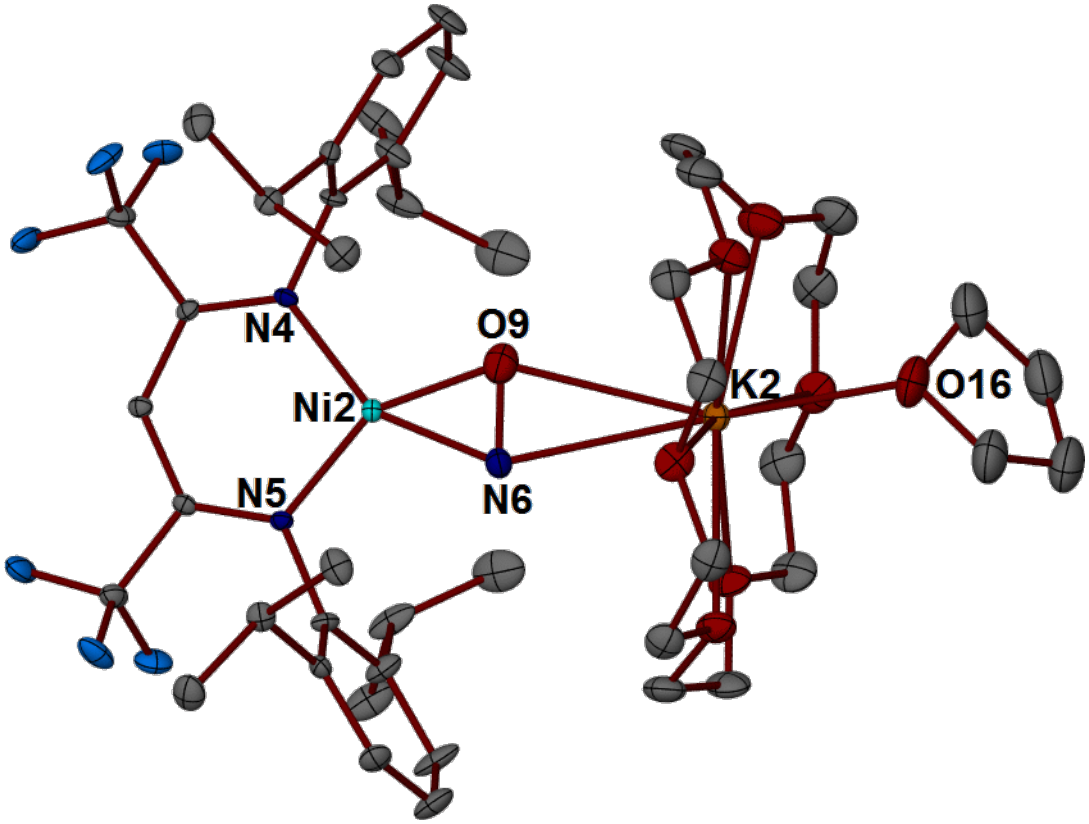

Figure S23b. X-ray structure of one of the two unique molecules of [^{i}Pr$_2$NN$_{F6}$]Ni(μ-η^2:η^2-NO)K[18-crown-6](THF) (**2a**) (CCDC 1565624) in the unit cell. The thermal ellipsoid plots are drawn at 30% probability level. Hydrogen atoms are omitted for clarity. Selected bond distances (Å) and angles (°) for molecule 2: Ni2-N4 1.874(4), Ni2-N5 1.880(4), Ni2-N6 1.866(5), Ni2-O9 1.868(5), N6-O9 1.284(6), Ni2•••K2 4.467, N4-Ni2-N5 99.63(18), N4-Ni2-O9 100.20 (2), N5-Ni2-N6 109.6(2), O9-Ni2-N6 40.2(2), Ni2-N6-O9 70.0(3).

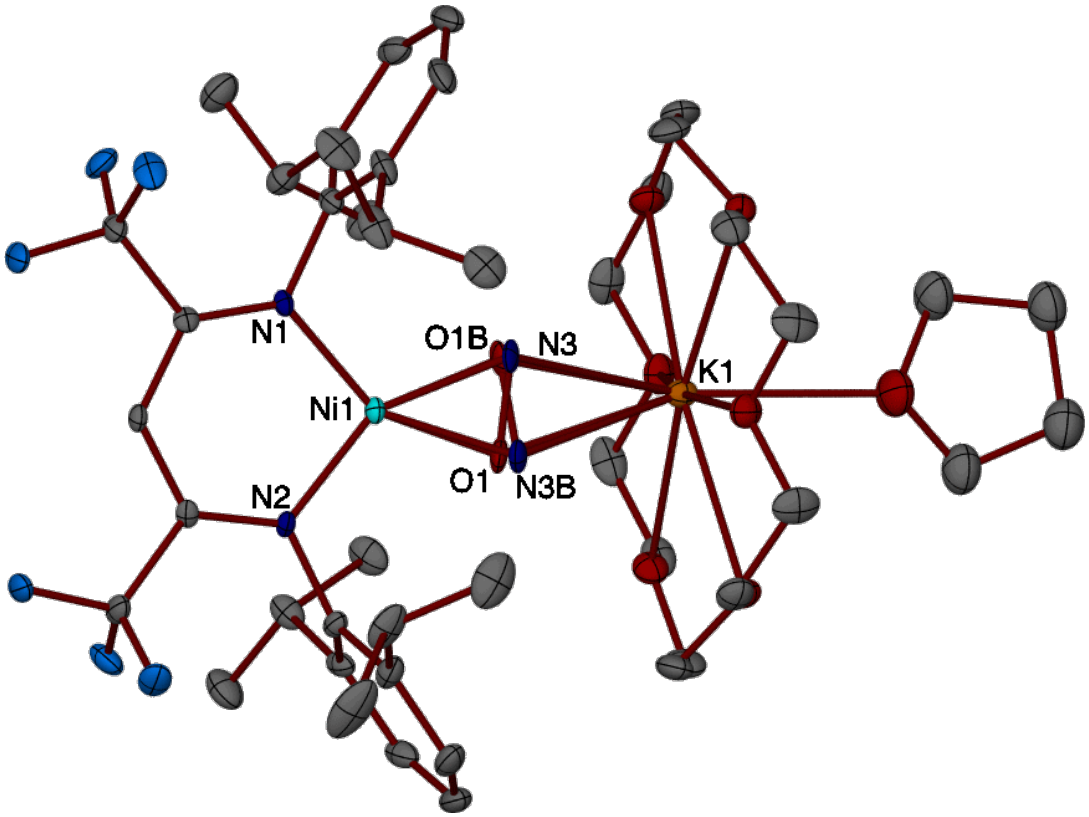

Figure S23c. Refinement of N/O positional disorder in molecule 1 of [^{i}Pr$_2$NN$_{F6}$]Ni(μ-η^2:η^2-NO)K[18-crown-6](THF) (**2a**) that results in two separate sets of positions for NO pairs in a 56:44 ratio. This model produces greater uncertainty in the N and O positions results in corresponding higher uncertainties in the bond distances and angles about the bridging NO ligand.

The thermal ellipsoid plots are drawn at 30% probability level. Hydrogen atoms are omitted for clarity. Selected bond distances (Å) and angles (°): Ni1-N1 1.865(4), Ni1-N2 1.864(4), Ni1-N3 1.89(4), Ni1-N3B 1.96(4), Ni1-O1 1.78(3), Ni1-O1B 1.81(3), N3-O1 1.32(7), N3B-O1B 1.28(10), Ni1•••K1 4.417, N1-Ni1-N2 99.63(18), N2-Ni1-O1 149.4(14), O1-Ni1-N3 42(2), N1-Ni1-N3 109.6(12), N2-Ni1-N3B 111.1(17), N3B-Ni1-O1B 40(3), O1B-Ni1-N1 110.7(14), Ni1-N3-O1 64(2), Ni1-N3B-O1B 64(3).

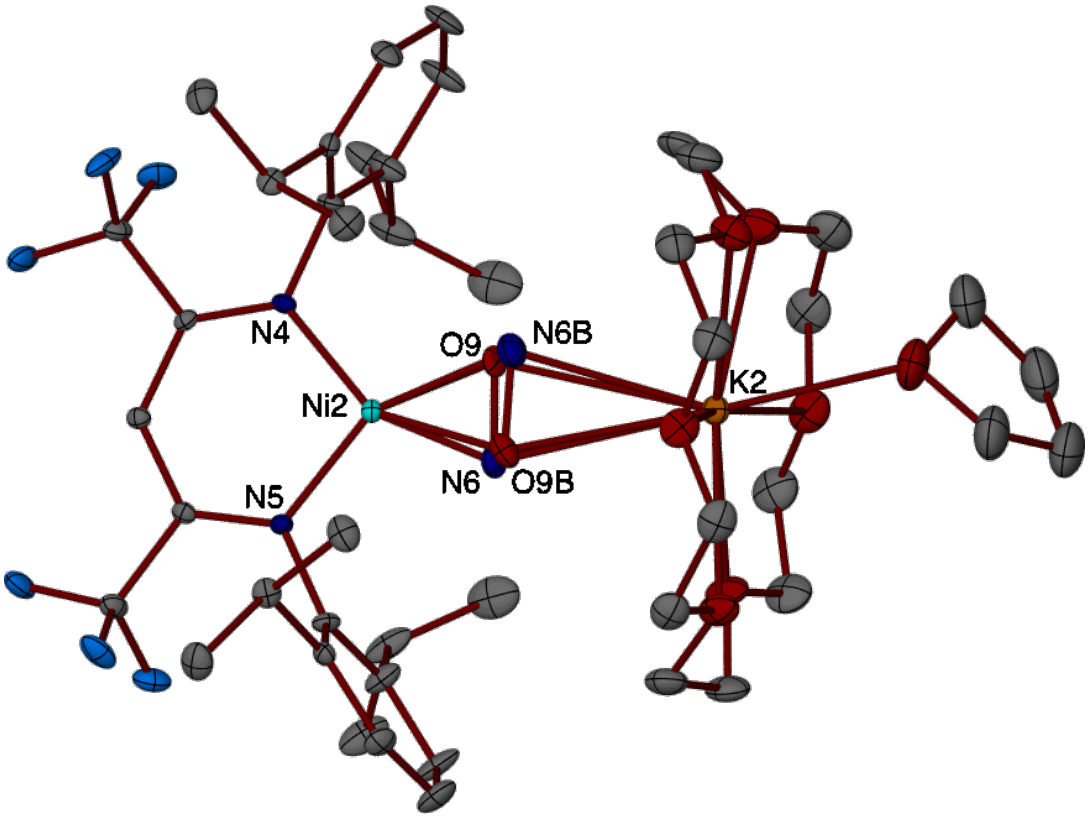

Figure S23d. Refinement of N/O positional disorder in molecule 2 of [^{i}Pr$_2$NN$_{F6}$]Ni(μ-η^2:η^2-NO)K[18-crown-6](THF) (**2a**) that results in two separate sets of positions for NO pairs in a 56:44 ratio. This model produces greater uncertainty in the N and O positions results in corresponding higher uncertainties in the bond distances and angles about the bridging NO ligand.

The thermal ellipsoid plots are drawn at 30% probability level. Hydrogen atoms are omitted for clarity. Selected bond distances (Å) and angles (°): Ni2-N4 1.874(4), Ni2-N5 1.880(4), Ni2-N6 1.80(4), Ni2-N6B 2.06(4), Ni2-O9 1.76(2), Ni2-O9B 1.93(4), N6-O9 1.306(18), Ni2•••K2 4.467, N4-Ni2-N5 100.19(18), N5-Ni2-N6 106.8(14), N6-Ni2-O9 43.0(9), N4-Ni2-O9 110.0(11), N5-Ni2-O9B 112.2(12), O9B-Ni2-N6b 37.9(8), N6B-Ni2-N4 109.5(15), Ni2-N6-O9 67.1(16), Ni2-N6B-O9B 66(2).

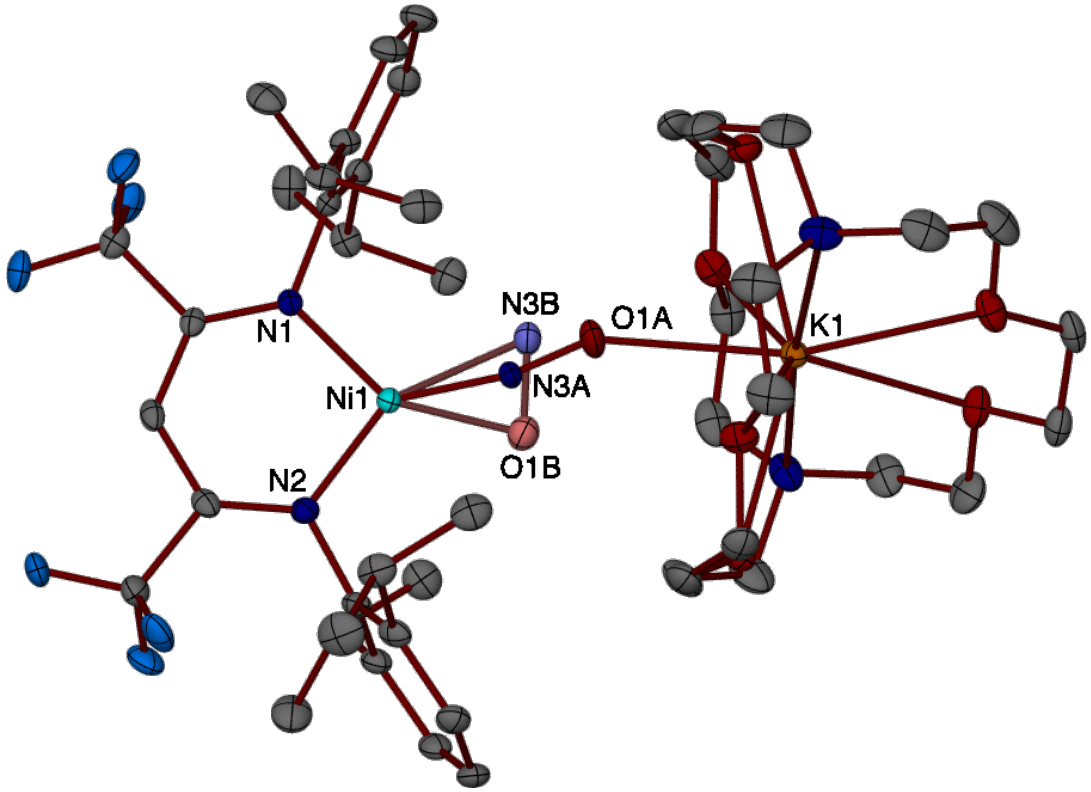

Figure S24. X-ray structure of [^{i}Pr$_2$NN$_{F6}$]Ni(μ-η^1:η^1-NO)K[2.2.2-cryptand] (**2b**) (CCDC 1565625). The nitrosyl ligand is disordered over three distinct orientations N3A-O1A, N3B-O1B, and N3C-O1C with 77%, 16%, and 7% site occupancies, respectively. Only the two major orientations N3A-O1A and N3B-O1B are shown for clarity. The thermal ellipsoid plots are drawn at 30% probability level. Hydrogen atoms are omitted for clarity. Selected bond distances (Å) and angles (°): Ni1-N1 1.8805(14), Ni1-N2 1.8828(15), Ni1-N3A 1.660(4), Ni1-N3B 2.04(2), Ni1-O1B 1.853(15), N3A-O1A 1.197(4), N3B-O1B 1.274(19), Ni1•••K1 5.466, N1-Ni1-N2 98.68(6), N1-Ni1-N3A 122.76(11), N2-Ni1-N3A 138.51(11), N1-Ni1- N3B 109.9(6), N2-Ni1- O1B 113.7(4), O1B-Ni1-N3B 37.8(6), Ni1-N3A-O1A 168.2(3), Ni1-N3B-O1B 63.1(12).

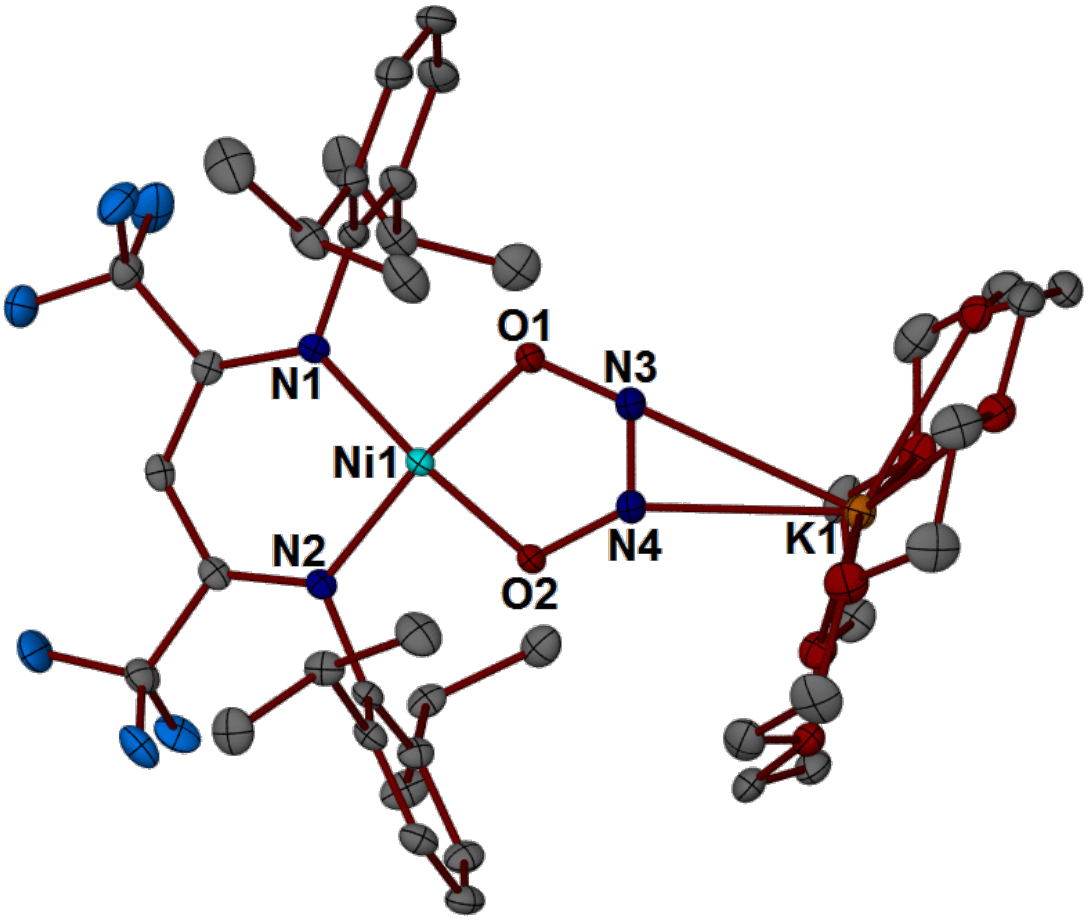

Figure S25. X-ray structure of [^{i}Pr$_2$NN$_{F6}$]Ni(κ^2-O$_2$N$_2$)K[18-crown-6] (**3a**) (CCDC 1565626). The thermal ellipsoid plots are drawn at 30% probability level. Hydrogen atoms are omitted for clarity. Selected bond distances (Å) and angles (°): Ni1-N1 1.8895(15), Ni1-N2 1.8936(15), Ni1-O1 1.8241(13), Ni1-O2 1.8187(13), Ni1-N3 2.669, Ni1-N4 2.669, O1-N3 1.370(2), N3-N4 1.235(2), N4-O2 1.367(2), N3-K1 2.7855(16), N4-K1 2.7519(17), Ni1•••K1 5.378, N1-Ni1-N2 96.52(7), N1-Ni1-O1 90.63(6), O1-Ni1-O2 83.16(6), N2-Ni1-O2 89.85(6).

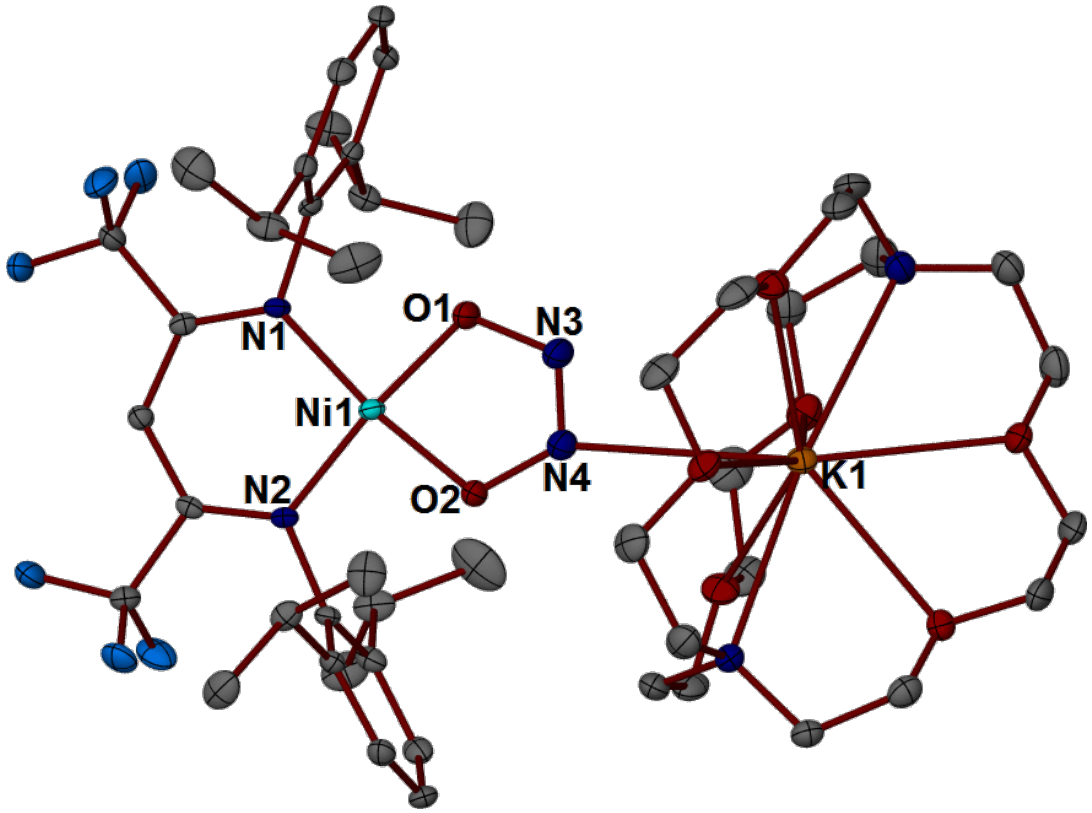

Figure S26. X-ray structure of [^{i}Pr$_2$NN$_{F6}$]Ni(κ^2-O$_2$N$_2$)K[2.2.2-cryptand] (**3b**) (CCDC 1565627). The thermal ellipsoid plots are drawn at 50% probability level. Hydrogen atoms are omitted for clarity. Selected bond distances (Å) and angles (°): Ni1-N1 1.8916(15), Ni1-N2 1.8996(15), Ni1-O1 1.8174(13), Ni1-O2 1.8233(13), Ni1-N3 2.682, Ni1-N4 2.684, O1-N3 1.373(2), N3-N4 1.235(2), N4-O2 1.375(2), N3-K1 3.628, N4-K1 3.274, Ni1•••K1 5.942, N1-Ni1-N2 96.52(6), N1-Ni1-O1 89.39(6), O1-Ni1-O2 82.61(6), N2-Ni1-O2 91.57(6).

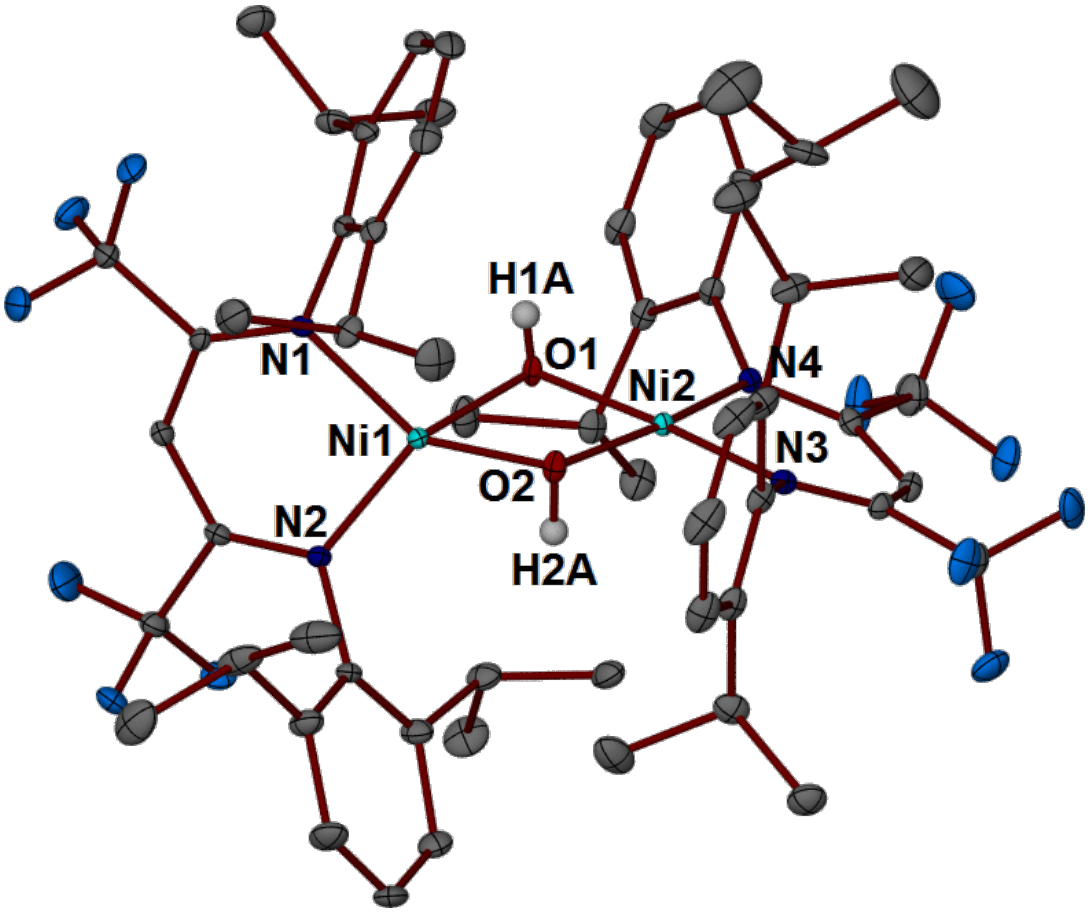

Figure S27. X-ray structure of $\{[^{i}Pr_2NN_{F6}]Ni\}_2(\mu\text{-}OH)_2$ (**4**) (CCDC 1565628). The thermal ellipsoid plots are drawn at 30% probability level. Hydrogen atoms are omitted for clarity. Selected bond distances (Å) and angles (°): Ni1-N1 1.9489(18), Ni1-N2 1.9377(18), Ni1-O1 1.9122(19), Ni1-O2 1.954(2), O1-Ni2 1.8705(19), O2-Ni2 1.8911(19), Ni2-N3 1.9127(18), Ni2-N4 1.9108(18), Ni1•••Ni2 2.966, N1-Ni1-N2 95.95(7), N1-Ni1-O1 106.63(8), O1-Ni1-O2 75.57(8), N2-Ni1-O2 122.31(8), N3-Ni2-N4 96.36(8), N3-Ni2-O2 93.54(8), O1-Ni2-O2 78.06(8)), N4-Ni2-O1 92.13(8). The bridging hydroxo groups are disordered over two positions.

12. XAS Details.

Ni K-edge XAS experiments were conducted on beamlines 9-3 (3 GeV, 60-100 mA) and 11-2 at the Stanford Synchrotron Radiation Lightsource (SSRL) under standard operating conditions. Beamline 9-3 is equipped with a 16-pole, 2.0 tesla wiggler, a liquid nitrogen-cooled double-crystal Si[220] monochromator, a Rh-coated harmonic rejection mirror and a cylindrical Rh-coated bent focusing mirror. A single energy was selected from the white beam with Si[220] ($\varphi = 0$) crystals. A liquid helium Oxford cryostat was attached to the beamline table to maintain a sample temperature of ~10 K. Beamline 11-2 is equipped with a 26-pole, 2.0 tesla wiggler, a liquid nitrogen-cooled double-crystal Si[220] monochromator and collimating and focusing mirrors. A single energy was selected from the white beam with Si[220] ($\varphi = 0$) crystals that were run de-tuned by 40% at 8700 eV. A liquid nitrogen-cooled cryostat was attached to the beamline table to maintain a sample temperature of 77 K. The table at both beamlines was equipped with three ionization chambers (under N_2 stream): I0 (10 cm, incident radiation), I1 (30 cm, transmission), and I2 (30 cm, calibration foil). The samples were measured exclusively in transmission mode with simultaneous measurement of the calibration foil. The energy was calibrated to a Ni foil, by setting the first inflection point to 8331.6 eV.

Ni samples were sealed in ampules for shipment to the synchrotron facility. The samples manipulated in an Ar glovebox at the synchrotron facility and diluted and finely ground with boron nitride such that the calculated edge jump for the absorbing atom would be at 1 absorption length in transmission mode. For BL9-3, samples were pressed into 1 mm aluminum holders and sealed with Kapton tape. For BL11-2, the ground solids were pressed with a teflon plug into an aluminum sample holder (8 slots) with one Kapton window superglued on the bottom (BL11-2). The samples were covered with a window of Kapton tape. This sample holder was nested inside a second aluminum sample holder and covered with Kapton windows that were sealed with indium wire. The samples were transferred to the beamline and immediately attached to the cold finger of a liquid N_2 cryostat, and quickly evacuated (10^{-5} Torr). Data were energy calibrated and normalized using Athena,[10] and fit using EXAFSPAK.[11] Fit intensities were multiplied by a factor of 100.

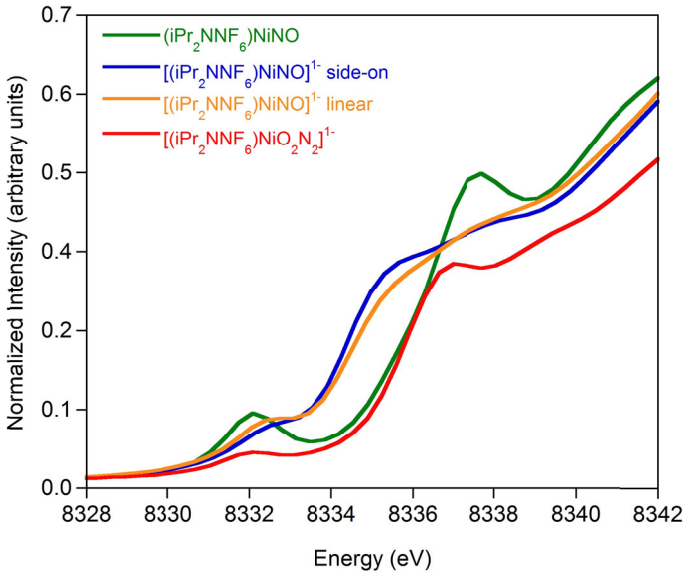

Figure S28. Normalized Ni K-edge X-ray absorption spectra of [^{i}Pr$_2$NN$_{F6}$]Ni complexes. Data collected at 77 K.

Table S2. Pre-edge energies (eV) and intensities determined from fits to experimental data. Intensities are calculated as in reference[12] and multiplied by 100. Errors are based on standard deviations of at least 3 fits.

Complex	Peak 1		Peak 2		Peak 3		Peak 4	
	eV	Int.	eV	Int.	eV	Int.	eV	Int.
[^{i}Pr$_2$NN$_{F6}$]NiNO (**1**)	8332.1	6.3(2)	8337.5	63(2)	8340.1(2)	11(6)	8341.7(4)	70(20)
[^{i}Pr$_2$NN$_{F6}$]Ni(μ-η^2:η^2-NO)K[18-crown-6](THF) (**2a**)	8332.3(1)	3.2(6)	8335.2(1)	18(4)	8337.3(2)	49(3)	8341.3(5)	90(10)
[^{i}Pr$_2$NN$_{F6}$]Ni(μ-η^1:η^1-NO)K[2.2.2-cryptand] (**2b**)	8332.3	3.9(7)	8335.2(1)	13(4)	8337.3(3)	42(3)	8341.2(7)	108(4)
[^{i}Pr$_2$NN$_{F6}$]Ni(κ^2-O$_2$N$_2$)K[18-crown-6] (**3a**)	8332.0	1.9(3)	8336.6	18	8338.8	49(4)	8342.2(2)	80(10)

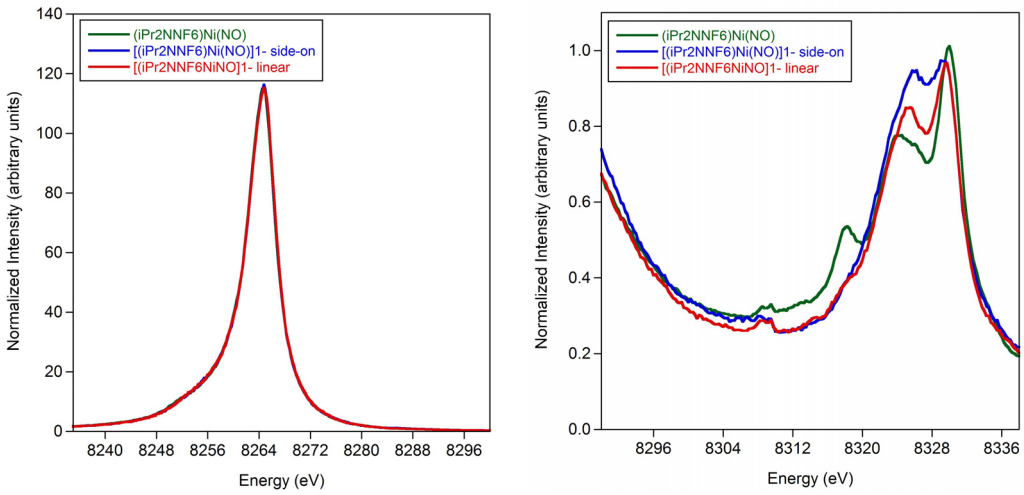

Figure S29. K β main line (left) and valence to core (right) XES spectra for [^{i}Pr$_2$NN$_{F6}$]Ni compounds at 10 K. The spectra of [^{i}Pr$_2$NN$_{F6}$]NiNO (**1**), [^{i}Pr$_2$NN$_{F6}$]Ni(μ-η^2:η^2-NO)K[18-crown-6] (**2a**), and [^{i}Pr$_2$NN$_{F6}$]Ni(μ-η^1:η^1-NO)K[2.2.2-cryptand] (**2b**) overlay in the K β main line.

13. Computational Details.

DFT calculations were conducted using the ORCA program[13] as previously described,[14] and using the XSEDE cluster.[15] Geometry optimizations were carried out at the B3LYP level of theory.[16,17,18] B3LYP is a hybrid-functional that has been shown to offer a more accurate description for metal-ligand bond lengths and interactions in transition metal compounds.[19] The all-electron Ahlrichs basis sets were applied,[20,21,22] utilizing triple-ξ def2-TZVP basis sets on the metal center and all atoms directly bound to the metal center. All other atoms were described using double-ξ def2-SV(P) basis sets. Auxiliary basis sets were selected to match the orbital basis.[23,24,25] The RIJCOSX approximation was used for computational expediency.[26,27,28] For broken symmetry calculations, the notation BS(x,y) signifies x spin up electrons and y spin down electrons.[29,30,31] The resulting coupled orbital pair was visualized by plotting the corresponding orbitals (uco). Orbitals and spin density plots were visualized using the program Chimera.[32] For complexes **2a** and **2b**, geometry optimizations were conducted on both the full molecule and the anion only. For the full molecule, it was necessary to fix the Ni-K distance, otherwise the linear conformation could not be isolated.

Surface scan calculations were conducted at the same level of theory as geometry optimizations. Scans were initiated with the geometry optimized structure from complex **2a** without the counter ion and the Ni-N-O angle was varied from 70-180° with 12 total sampling points. Results were consistent with full molecule calculations of complex **2a** starting with a Ni-N-O angle of 158.1° and decreasing the Ni-K distance. Attempts to include the K^+ counter ion and vary the Ni-K distance via lengthening or shortening, did not result in chemically reasonable conformations. Similarly, full molecule calculations starting with a Ni-N-O angle at 70° and successively increasing the Ni-K distance, did not result in any effect on the Ni-N-O angle.

XAS calculations were conducted as single-point calculations on the geometry optimized coordinates with the BP86 functional, the CP(PPP) basis set on nickel,[33] and the TZVP basis set on all other atoms.[34] The CP(PPP) basis set is based on the TurboMole DZ basis from the Ahlrichs group and utilizes Core-prop and polarization functions.[35] COSMO was applied to include a conductor-like infinite dielectric (ε=9.08)[36] and a dense integration grid with an integration accuracy of 7 was applied to increase radial integration accuracy. All

calculations were examined to ensure that the electronic structural description did not alter. To predict XAS pre-edge energies and intensities, TDDFT was used to examine quadrupole and magnetic dipole transitions with singlet excitations from Ni 1*s* orbitals.[37] The calculated energies for these compounds were shifted by 212.6 eV in this work by calibrating all compounds to a previously[3] reported compound [^{i}Pr$_2$NN$_{F6}$]Ni(μ-Br)Li(Et$_2$O)(dme), as we were not aware of a previous calibration study for Ni. The calculated spectra were plotted using the map_spc feature in the ORCA program over a range of 8000-9000 eV with 10,000 points and a weighting of 1.5 eV. The calculated pre-edge areas only included transitions that contained Ni *d*-character.

Table S3. Experimental and calculated bond distances (Å) and angles (degrees) resulting from geometry optimization.

	[^{i}Pr$_2$NN$_{F6}$]NiNO (1)		**{[^{i}Pr$_2$NN$_{F6}$]Ni (μ-η^2:η^2-NO)}$^{1-}$**		**{[^{i}Pr$_2$NN$_{F6}$]Ni (μ-η^1:η^1-NO)}$^{1-}$**		**{[^{i}Pr$_2$NN$_{F6}$]Ni (κ^2-O$_2$N$_2$)}$^{1-}$**	
Bond	Exp.	Exp.	Exp.	Calc.	Exp.	Calc.	Exp.	Calc.
N(1)=C(1)	1.3238(15)	1.322	1.329(2)	1.326	1.329(2)	1.323	1.323(2)	1.320
N(2)=C(3)	1.3249(15)	1.324	1.330(2)	1.327	1.330(2)	1.323	1.320(2)	1.320
C(1)-C(2)	1.3959(16)	1.405	1.392(3)	1.410	1.392(3)	1.410	1.386(3)	1.408
C(2)-C(3)	1.3966(16)	1.408	1.399(3)	1.411	1.399(3)	1.410	1.385(3)	1.407
Ni-N(1)	1.8899(10)	1.916	1.8805(14)	1.951	1.8805(14)	1.941	1.8895(15)	1.951
Ni-N(2)	1.8887(10)	1.925	1.8828(15)	1.916	1.8828(15)	1.949	1.8936(15)	1.950
Ni-O(1)	–	–	1.926(12)	1.910	–	–	1.8241(13)	1.836
Ni-O(2)	–	–	–	–	–	–	1.8187(13)	1.834
Ni-N(3)	1.6280(11)	1.634	1.916(9)	1.863	1.665(3)	1.755	–	–
O(1)-N(3)	1.1602(15)	1.154	1.289(14)	1.277	1.198(4)	1.215	1.370(2)	1.373
O(2)-N(4)	–	–	–	–	–	–	1.367(2)	1.370
N(3)-N(4)	–	–	–	–	–	–	1.235(2)	1.230
N(1)-Ni-N(2)	97.29(4)	97.7	98.68(6)	100.1	98.68(6)	97.9	96.52(7)	96.3
N(1)-Ni-O(1)	–	–	107.7(4)	112.8	–	–	90.63(6)	90.8
N(1)-Ni-N(3)	129.76(5)	125.1	–	–	123.78(12)	130.5	–	–
N(2)-Ni-N(3)	132.77(5)	137.1	–	–	137.49(12)	131.6	–	–
O(1)-Ni-O(2)	–	–	–	–	–	–	83.16(6)	82.2
N(2)-Ni-O(2)	–	–	–	–	–	–	89.85(6)	90.6

Table S4. Calculated relative energies (kcal/mol) resulting from anion only, $\{[^{i}Pr_2NN_{F6}]Ni(\mu\text{-}\eta^2\text{:}\eta^2\text{-}NO)\}^{1-}$, surface scans by fixing the Ni-N-O bond angle.

Ni-N-O angle (°)	Relative Energy (kcal/mol)
70	0
80	1.44
90	5.77
100	14.78
110	12.59
120	9.51
130	7.20
140	4.96

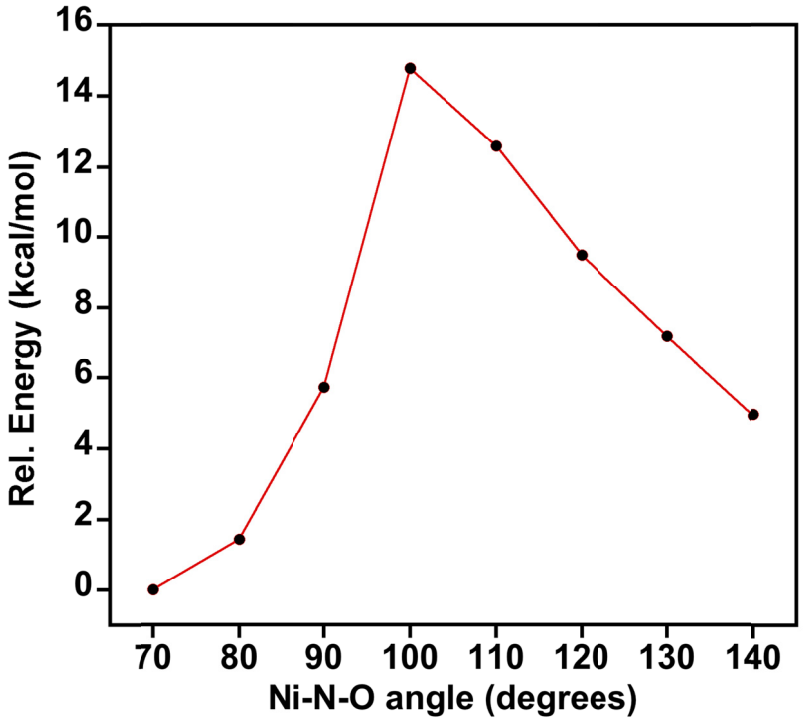

Figure S30. Calculated relative energies (kcal/mol) resulting from anion only, $\{[^{i}Pr_2NN_{F6}]Ni(\mu\text{-}\eta^2\text{:}\eta^2\text{-}NO)\}^{1-}$, surface scans by fixing the Ni-N-O bond angle.

Table S5. Calculated relative energies (kcal/mol) and angles (degrees) resulting from full molecule surface scans of [^{i}Pr$_2$NN$_{F6}$]Ni(μ-η^1:η^1-NO)K[2.2.2-cryptand] by shortening the Ni-K distance (Å).

Fixed Ni-K distance (Å)	Resulting Ni-N-O angle	Relative Energy (kcal/mol)
5.469	158.1	0.00
5.352	154.8	0.71
5.235	150.3	1.77
5.235	157.6	2.24
5.118	153.9	2.87
5.001	153	4.80
5.001	153.2	4.87
4.884	152.5	5.94
4.767	151	7.09
4.650	147.9	8.80
4.650	147.9	8.82
4.533	138.9	9.82
4.416	143	11.02
4.416	143.8	10.93

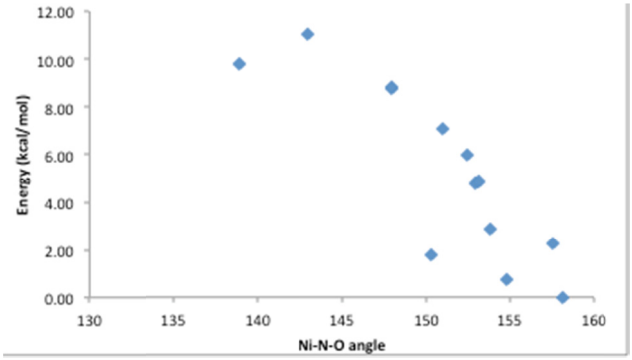

Figure S31. Calculated relative energies (kcal/mol) and angles (degrees) resulting from full molecule surface scans of [^{i}Pr$_2$NN$_{F6}$]Ni(μ-η^1:η^1-NO)K[2.2.2-cryptand] by shortening the Ni-K distance (Å).

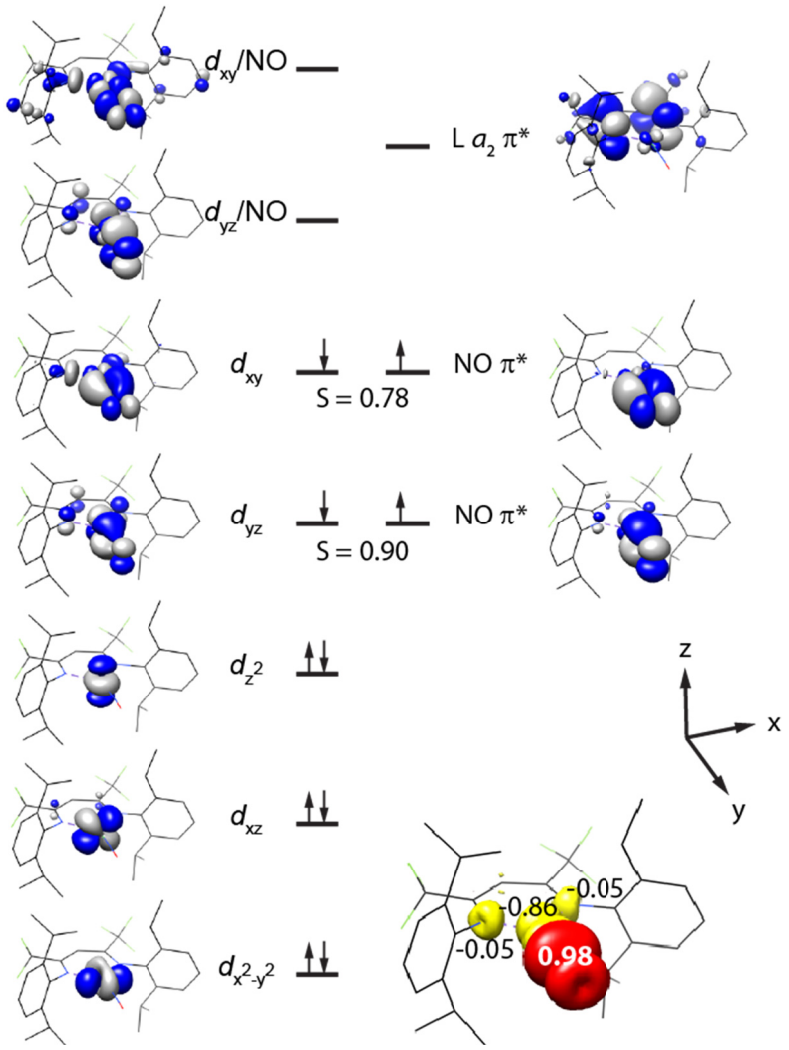

Figure S32. Qualitative *d*-orbital splitting diagram of localized canonical orbitals for [^{i}Pr$_2$NN$_{F6}$]NiNO (**1**) resulting from a BS(2,2) geometry optimization. Inset: Mulliken spin density plot where red is positive spin density and yellow is negative spin density.

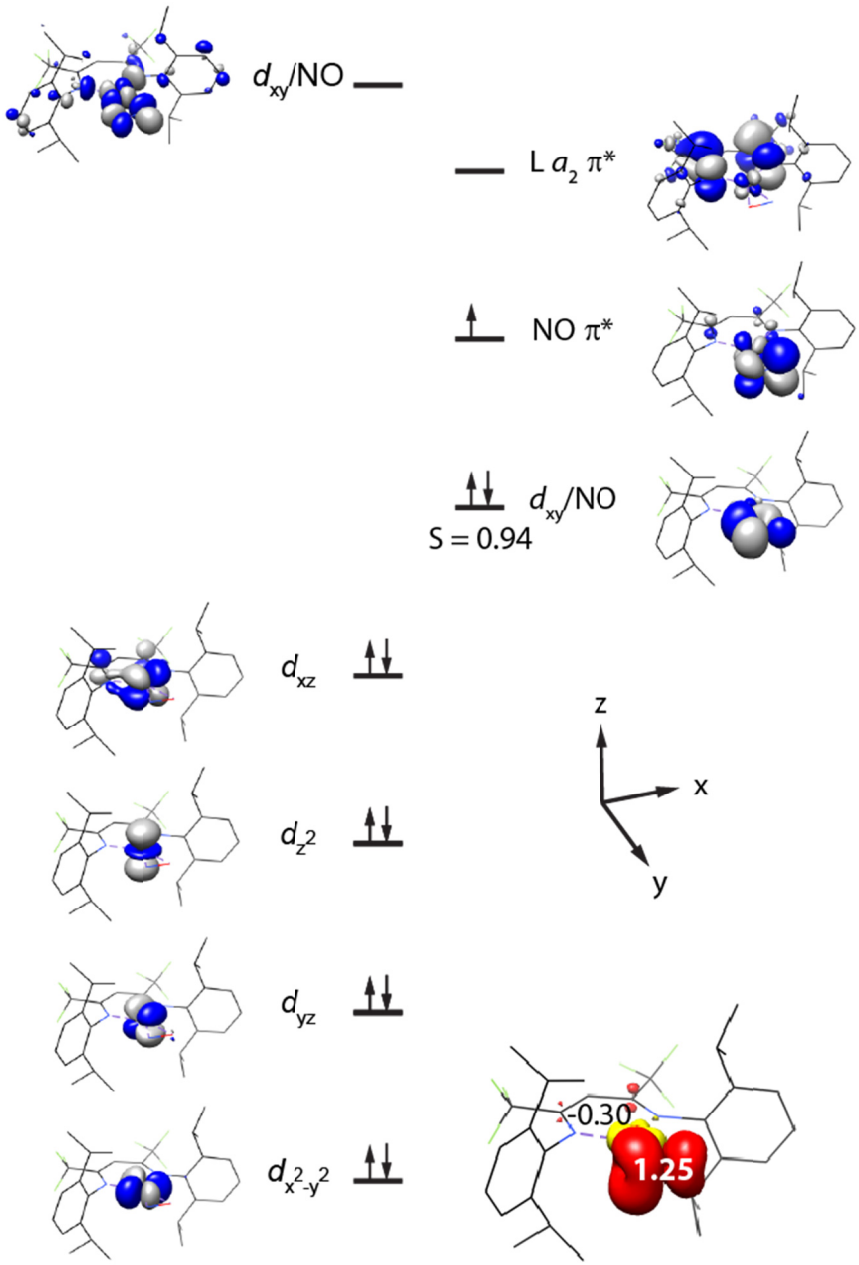

Figure S33. Qualitative *d*-orbital splitting diagram of localized canonical orbitals for {[^{i}Pr$_2$NN$_{F6}$]Ni(μ-η^2:η^2-NO)}$^{1-}$ resulting from a BS(2,1) geometry optimization. Inset: Mulliken spin density plot where red is positive spin density and yellow is negative spin density.

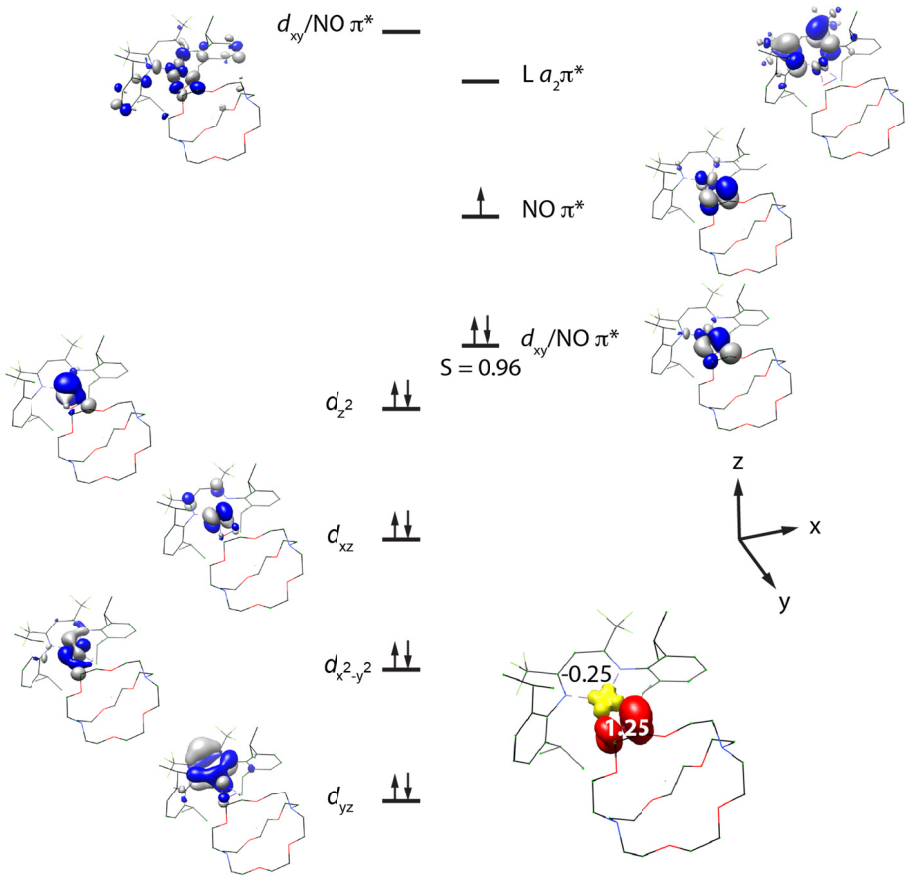

Figure S34. Qualitative *d*-orbital splitting diagram of localized canonical orbitals for [^{i}Pr$_2$NN$_{F6}$]Ni(μ-η^2:η^2-NO)K[2.2.2-cryptand] resulting from a BS(2,1) geometry optimization (fixed Ni-K distance of 5.466 Å). Inset: Mulliken spin density plot where red is positive spin density and yellow is negative spin density.

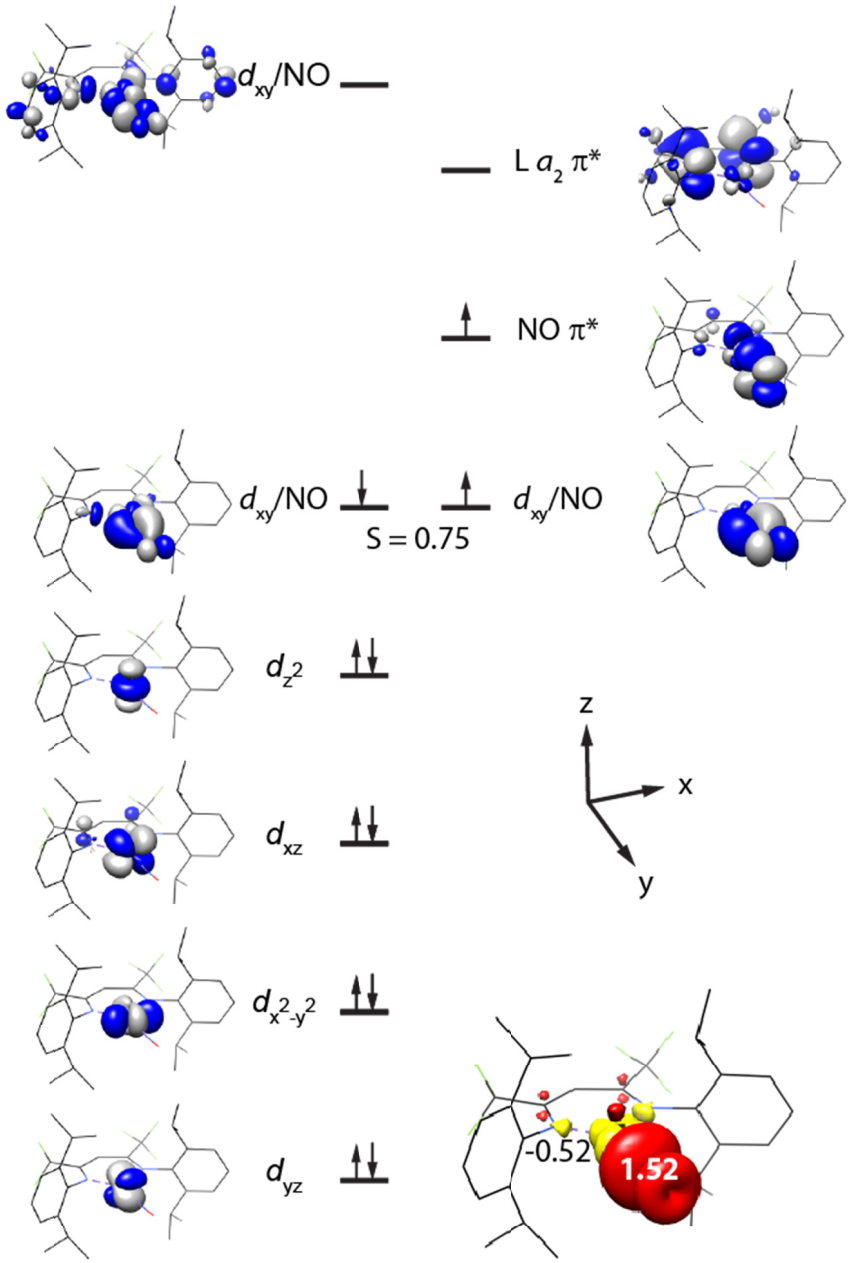

Figure S35. Qualitative *d*-orbital splitting diagram of localized canonical orbitals for $\{[^{i}Pr_2NN_{F6}]Ni(\mu\text{-}\eta^1\text{:}\eta^1\text{-}NO)\}^{1-}$ resulting from a UKS, S = ½ geometry optimization. Inset: Mulliken spin density plot where red is positive spin density and yellow is negative spin density.

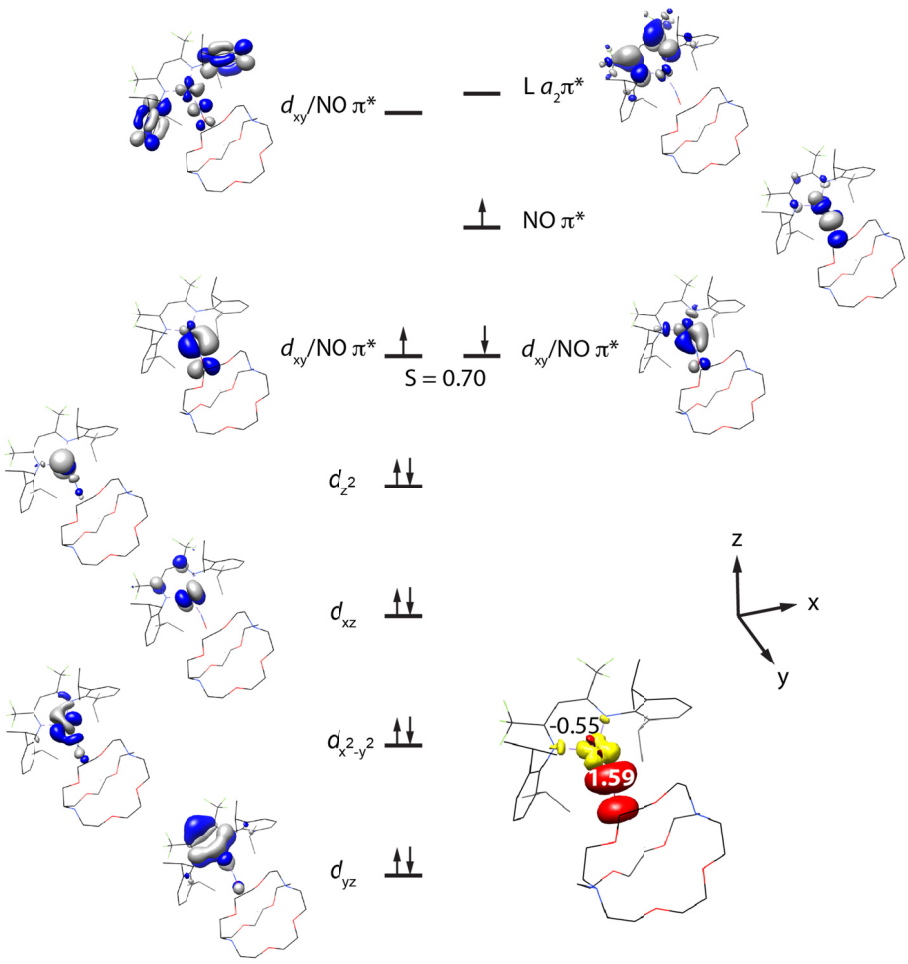

Figure S36. Qualitative *d*-orbital splitting diagram of localized canonical orbitals for [^{i}Pr$_2$NN$_{F6}$]Ni(μ-η^1:η^1-NO)K[2.2.2-cryptand] resulting from a BS(2,1) geometry optimization (fixed Ni-K distance of 5.466 Å). Inset: Mulliken spin density plot where red is positive spin density and yellow is negative spin density.

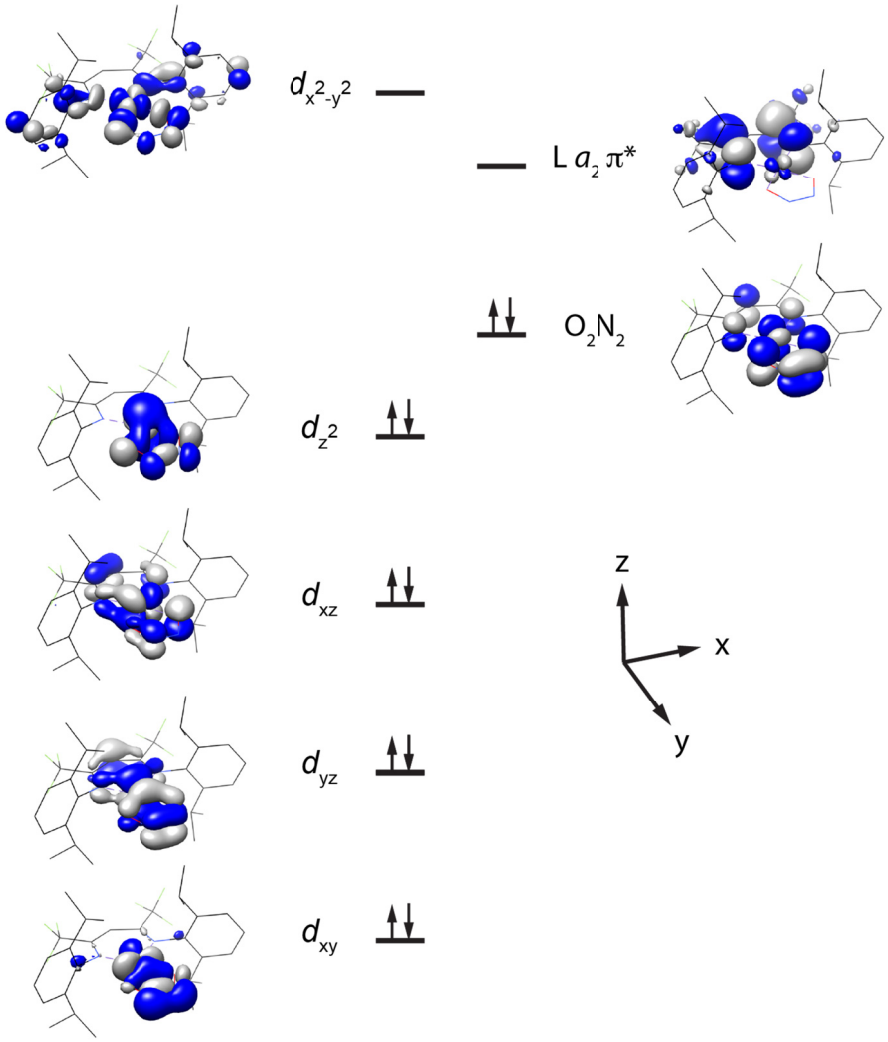

Figure S37. Qualitative *d*-orbital splitting diagram of localized canonical orbitals for $\{[^{i}Pr_2NN_{F6}]Ni(\kappa^2\text{-}O_2N_2)\}^{1-}$ resulting from a BS(2,1) geometry optimization.

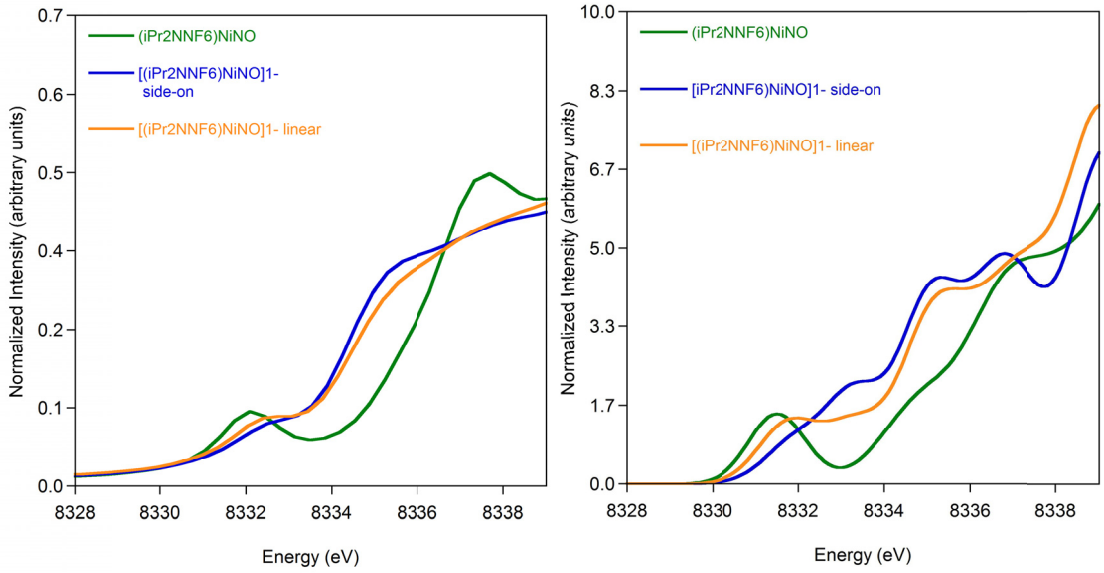

Figure S38. Experimental (left) versus TDDFT-calculated (right) pre-edge for [^{i}Pr$_2$NN$_{F6}$]NiNO (**1**), [^{i}Pr$_2$NN$_{F6}$]Ni(μ-η^2:η^2-NO)K(18-crown-6)(THF) (**2a**), [^{i}Pr$_2$NN$_{F6}$]Ni(μ-η^1:η^1-NO)K[2.2.2-cryptand] (**2b**). The calculated spectrum for **2b** consists of 77% linear and 23% side-on. A broadening of 1.5 eV and a shift of 212.6 eV have been applied to calculated spectra.

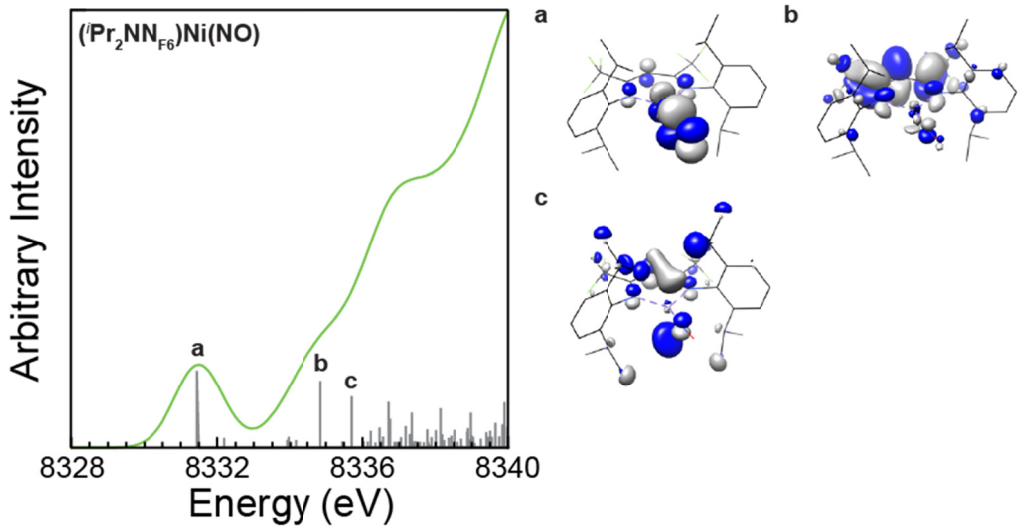

Figure S39. TDDFT-calculated pre-edge for [^{i}Pr$_2$NN$_{F6}$]NiNO (**1**) with molecular orbitals that contribute to calculated transitions. A broadening of 1.5 eV and a shift of 212.6 eV have been applied.

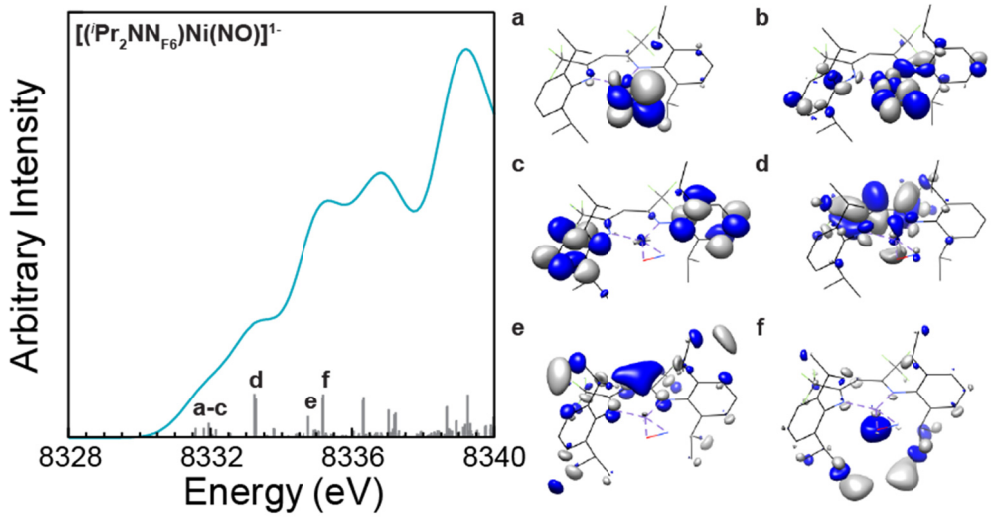

Figure S40. TDDFT-calculated pre-edge for $\{[^{i}Pr_2NN_{F6}]Ni(\mu\text{-}\eta^2\text{:}\eta^2\text{-NO})\}^{1-}$ with molecular orbitals that contribute to calculated transitions. A broadening of 1.5 eV and a shift of 212.6 eV have been applied.

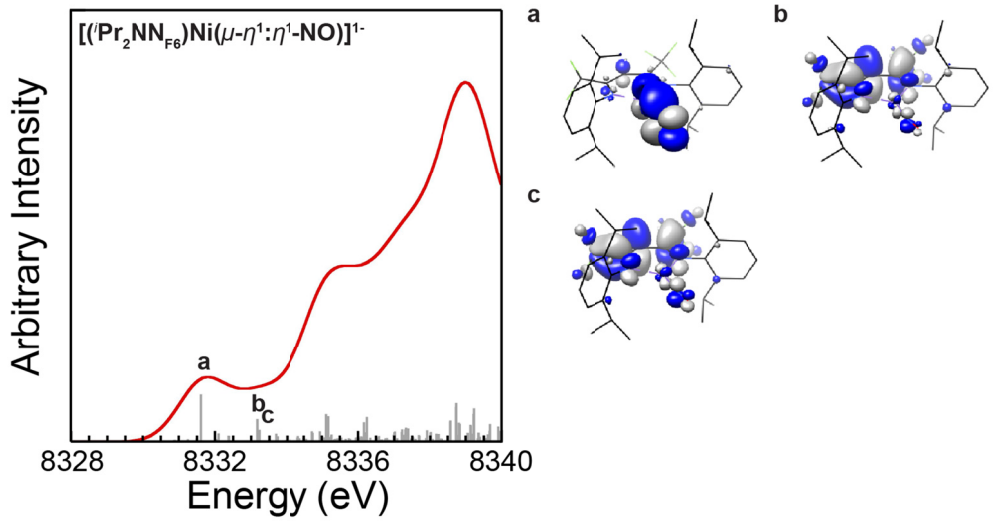

Figure S41. TDDFT-calculated pre-edge for $\{[^{i}Pr_2NN_{F6}]Ni(\mu\text{-}\eta^1\text{:}\eta^1\text{-NO})\}^{1-}$ with molecular orbitals that contribute to calculated transitions. A broadening of 1.5 eV and a shift of 212.6 eV have been applied.

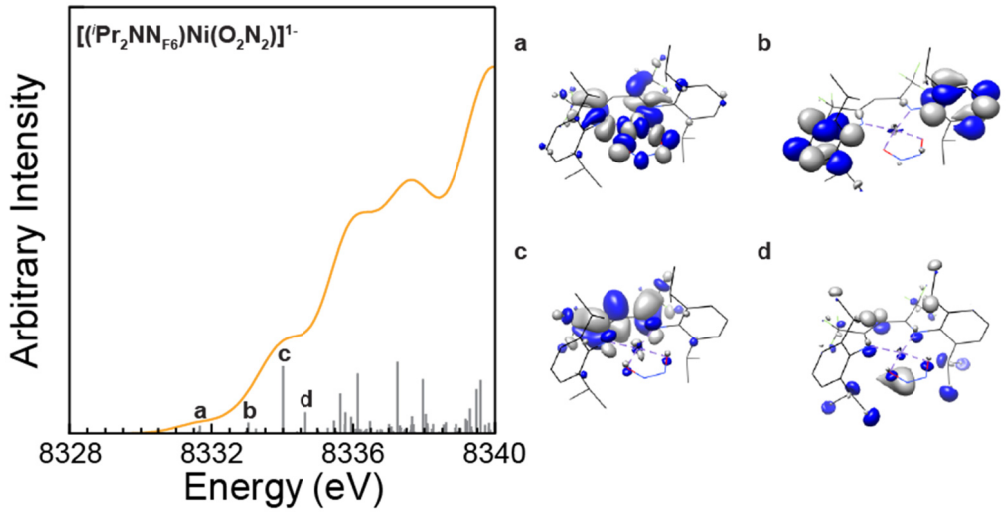

Figure S42. TDDFT-calculated pre-edge for $\{[^{i}Pr_2NN_{F6}]Ni(\kappa^2\text{-}O_2N_2)\}^{1-}$ with molecular orbitals that contribute to calculated transitions. A broadening of 1.5 eV and a shift of 212.6 eV have been applied.

Representative geometry optimization input file (ORCA):

```
! UKS B3LYP RIJCOSX SlowConv TightSCF def2-SV(P) def2-SVP/J
Normalprint UCO OPT

%basis NewGTO 28 "def2-TZVP(-f)" end
       NewGTO 7 "def2-TZVP(-f)" end
       NewGTO 8 "def2-TZVP(-f)" end
       NewAuxGTO 28 "def2-TZVP/J" end
       NewAuxGTO 7 "def2-TZVP/J" end
       NewAuxGTO 8 "def2-TZVP/J" end
       end

%scf   MaxIter 1000
       TolE 1E-7
       TolErr 1E-6
       end

* xyzfile 0 1 filename.xyz

%plots format cube
              dim1 100 dim2 100 dim3 100
              SpinDens("filename.cube");
              end
```

Representative orbital localization file using Pipek-Mezey localization (ORCA):

```
! UKS B3LYP RIJCOSX def2-SV(P) def2-SVP/J
! MORead noiter normalprint
! grid4 nofinalgrid
%moinp "geometryoptimizationfile.gbw"

%loc locmet pm end

* xyzfile 0 1 optimizedcoordinates.xyz
```

Representative surface scan input file (ORCA):

```
! UKS B3LYP RIJCOSX SlowConv TightSCF def2-SV(P) def2-SVP/J
Normalprint UCO OPT PAL8

%geom Scan
        A 0 2 1 = 70, 180, 12
        end
        end

%scf   Brokensym 2,1
        MaxIter 1000
      TolE 1E-7
      TolErr 1E-6
      End

* xyzfile 0 1 optimizedcoordinates.xyz
```

Representative TDDFT input file (ORCA):

```
! UKS BP86 TZVP def2-TZV/J TightSCF SlowConv COSMO SCFConv7
! Normalprint
! grid4 nofinalgrid

%basis  newgto Ni "CP(PPP)" end
    end

%method     SpecialGridAtoms 28
            SpecialGridIntAcc 7
            end

%scf   MaxIter 1000
            TolE 1e-7
            TolErr 1e-6
```

```
                end

* xyzfile 0 1 optimizedcoordinates.xyz

%tddft          orbwin[0] = 0,0,-1,-1
                orbwin[1] = 0,0,-1,-1
                doquad true
                maxdim 450
                maxcore 1500
                nroots 400
                triplets false
                end

%plots format cube
                dim1 100 dim2 100 dim3 100
                SpinDens("filename.cube");
                end
```

Geometry optimized coordinates (xyz format):

[^{i}Pr$_2$NN$_{F6}$]NiNO (**1**)

Ni	0.120	0.083	-0.059
O	-1.442	0.349	-2.419
N	-0.846	0.227	-1.431
N	2.039	-0.014	0.035
N	-0.213	0.017	1.837
F	4.810	0.914	0.834
F	1.497	-0.129	5.019
F	4.744	-0.630	2.337
F	-0.117	1.222	4.535
F	4.681	-1.171	0.255
F	-0.471	-0.914	4.638
C	3.001	1.434	-1.709
C	2.707	-0.158	1.165
C	0.750	-0.064	2.741
C	0.410	0.020	4.245
C	4.247	-0.266	1.146
C	2.120	-0.177	2.443
C	2.755	-0.997	-2.110
C	2.652	0.135	-1.264
C	-1.622	0.036	2.158
C	2.336	-2.397	-1.661
C	2.822	2.678	-0.836
C	-2.315	1.271	2.179
C	-3.701	1.245	2.400
C	3.595	0.469	-3.869
C	3.241	-0.800	-3.410
C	-3.689	-1.163	2.528
C	-2.304	-1.198	2.318
C	3.471	1.571	-3.024
C	1.082	-2.890	-2.413
C	-4.386	0.044	2.573
C	-1.592	-2.545	2.192
C	1.571	3.477	-1.252
C	-1.893	-3.191	0.822
C	3.479	-3.422	-1.783
C	-1.907	-3.520	3.340
C	4.066	3.584	-0.813
C	-1.626	2.611	1.917
C	-2.039	3.191	0.548

C	-1.871	3.637	3.037
H	2.795	-0.272	3.287
H	-5.468	0.048	2.744
H	-4.257	2.187	2.428
H	-4.236	-2.101	2.658
H	-2.968	-3.828	3.350
H	-1.302	-4.438	3.233
H	-2.936	3.928	3.102
H	-1.291	4.557	2.843
H	3.918	4.408	-0.091
H	4.261	4.049	-1.797
H	4.372	-3.094	-1.227
H	3.774	-3.585	-2.836
H	0.244	-2.178	-2.320
H	0.747	-3.861	-2.003
H	-1.566	3.238	4.019
H	-1.672	-3.069	4.320
H	3.158	-4.398	-1.374
H	-2.967	-3.435	0.720
H	-1.623	-2.514	-0.009
H	-1.318	-4.126	0.700
H	-3.114	3.447	0.526
H	-1.470	4.112	0.327
H	-1.851	2.473	-0.269
H	3.748	2.561	-3.397
H	3.975	0.600	-4.887
H	3.346	-1.659	-4.080
H	1.285	-3.031	-3.490
H	2.068	-2.340	-0.594
H	2.656	2.344	0.200
H	-0.508	-2.361	2.226
H	-0.539	2.430	1.880
H	4.967	3.025	-0.513
H	1.434	4.352	-0.591
H	1.654	3.848	-2.290
H	0.657	2.860	-1.186

{[^{i}Pr$_2$NN$_{F6}$]Ni(μ-η^2:η^2-NO)}$^{1-}$ side-on

Ni	-0.216	-0.078	-0.182
O	-1.669	-0.810	0.816
N	-0.148	1.870	-0.101
N	-0.976	-1.722	0.253
N	1.318	-0.421	-1.279
F	-0.306	4.628	-1.267
F	1.840	4.605	-1.425
F	0.923	4.541	0.518
F	2.962	-0.332	-3.809
F	3.948	1.400	-2.990
F	4.164	-0.509	-2.020
C	-2.364	2.918	0.223
C	-1.106	2.521	0.746
C	-3.285	3.534	1.083
C	0.808	4.071	-0.741
C	-0.819	2.693	2.126
C	0.772	2.536	-0.786
C	0.471	2.175	2.762
C	-1.773	3.320	2.940
C	-2.996	3.751	2.428
C	-2.770	2.621	-1.218
C	1.224	3.261	3.552
C	-3.423	3.824	-1.924
C	0.179	0.949	3.651
C	1.773	1.948	-1.585
C	1.678	-1.801	-1.448
C	-3.691	1.384	-1.256
C	1.147	-2.546	-2.532
C	1.518	-3.893	-2.662
C	-1.290	-2.432	-3.217
C	3.272	0.282	-2.647
C	2.498	-2.430	-0.474
C	2.036	0.575	-1.780
C	2.973	-1.693	0.778
C	2.838	-3.777	-0.651
C	2.231	-2.205	2.030
C	0.143	-1.939	-3.511
C	4.496	-1.751	0.987
C	2.372	-4.506	-1.746
C	0.491	-2.189	-4.989
H	-1.552	3.476	4.001
H	-0.476	1.221	4.500

H	-4.256	3.850	0.688
H	1.118	0.534	4.066
H	-0.325	0.156	3.072
H	-1.859	2.365	-1.781
H	1.464	4.127	2.912
H	2.171	2.856	3.955
H	0.635	3.627	4.413
H	1.132	1.836	1.950
H	-4.393	4.095	-1.465
H	-3.728	4.241	3.080
H	-3.626	3.582	-2.984
H	-2.769	4.712	-1.890
H	2.445	2.635	-2.084
H	-4.639	1.585	-0.721
H	-3.206	0.518	-0.772
H	-3.942	1.109	-2.298
H	1.124	-4.477	-3.500
H	2.702	-0.633	0.658
H	3.482	-4.268	0.087
H	2.483	-3.263	2.237
H	2.513	-1.607	2.917
H	1.138	-2.133	1.893
H	0.153	-0.850	-3.349
H	5.040	-1.378	0.103
H	4.784	-1.123	1.852
H	4.849	-2.778	1.200
H	2.667	-5.553	-1.880
H	0.384	-3.257	-5.260
H	-0.196	-1.621	-5.642
H	1.522	-1.874	-5.226
H	-1.390	-3.510	-3.452
H	-1.552	-2.284	-2.155
H	-2.021	-1.882	-3.841

[^{i}Pr$_2$NN$_{F6}$]Ni(μ-η^2:η^2-NO)K[2.2.2-cryptand] side-on

Ni	-0.269	-0.023	0.070
K	-0.044	-5.480	0.292
O	-0.909	-1.795	-0.131
N	0.301	-1.779	0.321
O	0.474	-4.763	-2.277
O	2.634	-4.836	-0.412
O	-1.054	-8.238	-0.919
O	0.856	-8.366	1.316

O	-2.682	-4.743	1.061
O	-0.487	-4.785	2.918
N	-1.604	1.289	-0.533
N	1.139	1.194	0.571
N	-2.318	-5.658	-1.814
N	2.226	-5.899	2.409
C	-1.349	2.586	-0.500
C	-0.182	3.168	0.038
H	-0.150	4.252	0.050
C	0.965	2.508	0.520
C	-2.377	3.604	-1.037
F	-1.866	4.838	-1.182
F	-2.862	3.259	-2.242
F	-3.434	3.729	-0.206
C	2.086	3.446	1.009
F	1.722	4.740	1.006
F	3.200	3.367	0.254
F	2.452	3.159	2.273
C	-2.818	0.732	-1.065
C	-3.962	0.595	-0.234
C	-5.093	-0.056	-0.752
H	-5.981	-0.164	-0.121
C	-5.114	-0.563	-2.050
H	-6.009	-1.064	-2.437
C	-3.988	-0.411	-2.859
H	-4.010	-0.798	-3.883
C	-2.833	0.233	-2.395
C	2.427	0.610	0.845
C	3.348	0.451	-0.225
C	4.568	-0.192	0.030
H	5.289	-0.315	-0.785
C	4.892	-0.663	1.303
H	5.856	-1.149	1.486
C	3.984	-0.487	2.346
H	4.253	-0.838	3.348
C	2.747	0.146	2.147
C	-4.002	1.104	1.208
H	-3.152	1.784	1.352
C	-1.642	0.381	-3.343
H	-0.874	0.973	-2.823
C	3.040	0.944	-1.640
H	2.200	1.651	-1.576
C	1.796	0.317	3.331

H	0.997	1.003	3.011
C	-3.827	-0.046	2.217
H	-4.645	-0.785	2.123
H	-3.842	0.349	3.251
H	-2.869	-0.573	2.058
C	-5.285	1.899	1.526
H	-5.480	2.672	0.766
H	-5.190	2.401	2.507
H	-6.173	1.242	1.584
C	-1.009	-0.986	-3.674
H	-0.705	-1.508	-2.752
H	-0.116	-0.852	-4.312
H	-1.719	-1.634	-4.224
C	-2.011	1.137	-4.636
H	-2.728	0.566	-5.254
H	-1.109	1.310	-5.253
H	-2.465	2.116	-4.412
C	2.572	-0.209	-2.545
H	3.379	-0.953	-2.696
H	2.278	0.179	-3.539
H	1.700	-0.725	-2.108
C	4.212	1.702	-2.291
H	5.053	1.029	-2.542
H	4.597	2.500	-1.634
H	3.877	2.171	-3.235
C	1.124	-1.017	3.716
H	0.642	-1.484	2.840
H	0.360	-0.850	4.499
H	1.870	-1.725	4.128
C	2.483	0.947	4.560
H	3.220	0.261	5.018
H	1.733	1.184	5.337
H	3.009	1.880	4.298
C	-1.867	-4.698	-2.832
H	-1.908	-3.692	-2.387
H	-2.551	-4.695	-3.712
C	-0.446	-4.899	-3.348
H	-0.310	-5.879	-3.851
H	-0.260	-4.114	-4.108
C	1.822	-4.501	-2.654
H	1.851	-3.776	-3.493
H	2.321	-5.435	-2.985
C	2.547	-3.884	-1.475

H	3.565	-3.579	-1.794
H	2.001	-2.985	-1.133
C	3.237	-4.277	0.757
H	2.606	-3.456	1.148
H	4.220	-3.836	0.496
C	3.457	-5.389	1.774
H	3.947	-6.220	1.242
H	4.176	-5.030	2.544
C	-2.519	-6.999	-2.373
H	-1.751	-7.184	-3.140
H	-3.506	-7.080	-2.884
C	-2.406	-8.126	-1.356
H	-3.069	-7.959	-0.483
H	-2.724	-9.073	-1.842
C	-0.833	-9.362	-0.081
H	-1.058	-10.297	-0.637
H	-1.496	-9.326	0.809
C	0.614	-9.395	0.367
H	0.828	-10.385	0.825
H	1.277	-9.273	-0.515
C	2.215	-8.325	1.743
H	2.874	-8.105	0.879
H	2.512	-9.317	2.146
C	2.378	-7.291	2.848
H	1.611	-7.508	3.606
H	3.366	-7.453	3.340
C	-3.540	-5.169	-1.147
H	-4.043	-6.026	-0.673
H	-4.251	-4.749	-1.895
C	-3.311	-4.122	-0.067
H	-2.695	-3.277	-0.420
H	-4.294	-3.711	0.239
C	-2.553	-3.845	2.164
H	-3.557	-3.527	2.515
H	-1.994	-2.943	1.853
C	-1.831	-4.530	3.306
H	-1.851	-3.855	4.185
H	-2.340	-5.476	3.584
C	0.378	-5.166	3.977
H	0.137	-6.193	4.321
H	0.234	-4.490	4.843
C	1.826	-5.027	3.522
H	1.961	-3.982	3.202

H	2.485	-5.185	4.408

{[^{i}Pr$_2$NN$_{F6}$]Ni(μ-η^1:η^1-NO)}$^{1-}$ linear:

Ni	-0.047	0.180	0.017
N	-1.189	0.508	-1.274
N	-0.344	-0.255	1.885
N	1.902	0.157	0.044
O	-1.942	0.574	-2.225
F	-0.569	0.121	4.752
F	1.456	-0.568	5.007
F	-0.076	-1.956	4.390
F	4.679	1.046	0.728
F	4.583	-1.066	0.267
F	4.674	-0.405	2.316
C	-1.717	-0.482	2.219
C	-2.242	-1.800	2.154
C	-2.567	0.619	2.506
C	2.655	-0.698	-2.138
C	2.854	1.705	-1.619
C	0.652	-0.375	2.747
C	2.590	-0.070	1.151
C	2.022	-0.279	2.425
C	-2.057	2.059	2.490
C	2.507	0.384	-1.232
C	2.584	2.894	-0.700
C	-3.920	0.368	2.769
C	-2.608	2.830	1.273

C	3.578	0.846	-3.785
C	0.366	-0.689	4.220
C	3.389	1.907	-2.899
C	-4.440	-0.927	2.752
C	4.126	-0.122	1.116
C	3.204	-0.443	-3.403
C	-3.600	-1.996	2.440
C	-1.390	-2.978	1.681
C	0.957	-2.503	-2.649
C	-1.496	-4.223	2.578
C	-2.346	2.811	3.804
C	-1.722	-3.322	0.214
C	3.280	-3.168	-1.869
C	2.171	-2.104	-1.788
C	1.287	3.621	-1.111
C	3.766	3.874	-0.604
H	1.377	4.060	-2.124
H	1.064	4.442	-0.403
H	0.430	2.925	-1.111
H	4.692	3.354	-0.302
H	3.552	4.655	0.149
H	3.960	4.393	-1.562
H	1.821	-2.076	-0.746
H	3.659	-3.294	-2.901
H	2.888	-4.149	-1.538
H	4.135	-2.906	-1.225
H	-2.765	-3.680	0.113

H	-1.052	-4.119	-0.160
H	-1.596	-2.436	-0.433
H	-3.430	2.951	3.971
H	-1.885	3.816	3.776
H	-1.933	2.271	4.672
H	-4.586	1.208	2.994
H	2.717	-0.413	3.245
H	-0.962	2.019	2.370
H	2.413	2.497	0.312
H	-2.374	2.297	0.335
H	-2.153	3.838	1.218
H	-3.706	2.956	1.337
H	4.012	1.027	-4.774
H	3.668	2.918	-3.214
H	-5.498	-1.104	2.974
H	3.336	-1.272	-4.107
H	-4.019	-3.007	2.400
H	-0.339	-2.656	1.702
H	0.156	-1.747	-2.577
H	0.543	-3.470	-2.303
H	1.236	-2.614	-3.715
H	-2.509	-4.668	2.559
H	-1.244	-3.985	3.625
H	-0.794	-5.002	2.226

[^{i}Pr$_2$NN$_{F6}$]Ni(μ-η^1:η^1-NO)K[2.2.2-cryptand] linear

Ni	0.106	0.015	0.263
K	-0.358	-5.414	-0.177
O	-0.217	-2.819	-0.365

N	-0.076	-1.734	0.196
O	-0.611	-4.884	-2.940
O	2.017	-5.101	-1.737
O	-1.250	-8.248	-0.901
O	0.959	-7.940	0.964
O	-2.823	-5.197	1.289
O	-0.331	-4.492	2.442
N	-1.277	1.236	-0.405
N	1.419	1.353	0.829
N	-3.043	-5.902	-1.649
N	2.274	-5.276	1.289
C	-1.095	2.547	-0.399
C	0.046	3.214	0.094
H	0.031	4.297	0.023
C	1.203	2.648	0.670
C	-2.198	3.475	-0.944
F	-1.832	4.767	-0.971
F	-2.559	3.156	-2.202
F	-3.316	3.414	-0.191
C	2.277	3.662	1.106
F	1.876	4.938	0.984
F	3.398	3.544	0.364
F	2.644	3.502	2.393
C	-2.418	0.585	-0.989
C	-3.574	0.306	-0.209
C	-4.608	-0.449	-0.787
H	-5.501	-0.671	-0.194
C	-4.529	-0.918	-2.098
H	-5.354	-1.496	-2.531
C	-3.396	-0.624	-2.857
H	-3.339	-0.979	-3.891
C	-2.333	0.124	-2.332
C	2.565	0.793	1.491
C	3.722	0.424	0.752
C	4.741	-0.280	1.414
H	5.634	-0.578	0.854
C	4.649	-0.605	2.767
H	5.460	-1.151	3.262
C	3.523	-0.205	3.488
H	3.462	-0.443	4.555
C	2.475	0.501	2.881
C	-3.739	0.777	1.236
H	-2.947	1.510	1.446

C	-1.125	0.413	-3.226
H	-0.451	1.081	-2.667
C	3.906	0.762	-0.729
H	3.109	1.465	-1.013
C	1.271	0.922	3.726
H	0.658	1.603	3.118
C	-3.556	-0.380	2.234
H	-4.314	-1.170	2.071
H	-3.672	-0.012	3.272
H	-2.556	-0.838	2.135
C	-5.094	1.475	1.482
H	-5.286	2.261	0.735
H	-5.106	1.945	2.484
H	-5.937	0.759	1.450
C	-0.329	-0.870	-3.537
H	-0.034	-1.396	-2.613
H	0.583	-0.623	-4.112
H	-0.930	-1.571	-4.149
C	-1.516	1.136	-4.532
H	-2.131	0.491	-5.187
H	-0.612	1.418	-5.104
H	-2.091	2.055	-4.328
C	3.753	-0.476	-1.630
H	4.508	-1.246	-1.384
H	3.894	-0.192	-2.691
H	2.750	-0.927	-1.520
C	5.256	1.456	-1.007
H	6.106	0.756	-0.902
H	5.424	2.302	-0.321
H	5.280	1.846	-2.042
C	0.379	-0.284	4.081
H	0.047	-0.813	3.170
H	-0.519	0.051	4.633
H	0.923	-1.002	4.726
C	1.676	1.690	5.000
H	2.225	1.047	5.713
H	0.778	2.066	5.525
H	2.318	2.554	4.760
C	-3.015	-4.922	-2.743
H	-3.022	-3.916	-2.293
H	-3.933	-5.004	-3.376
C	-1.813	-5.016	-3.676
H	-1.812	-5.969	-4.243

H	-1.896	-4.198	-4.423
C	0.562	-5.176	-3.687
H	0.483	-4.751	-4.709
H	0.692	-6.275	-3.780
C	1.767	-4.540	-3.024
H	2.652	-4.700	-3.677
H	1.585	-3.452	-2.936
C	2.853	-4.248	-0.947
H	2.301	-3.324	-0.698
H	3.749	-3.960	-1.534
C	3.325	-4.984	0.299
H	3.773	-5.932	-0.036
H	4.146	-4.391	0.759
C	-3.109	-7.285	-2.129
H	-2.453	-7.386	-3.006
H	-4.137	-7.554	-2.469
C	-2.655	-8.337	-1.124
H	-3.190	-8.240	-0.159
H	-2.901	-9.337	-1.542
C	-0.785	-9.268	-0.027
H	-0.969	-10.266	-0.480
H	-1.326	-9.224	0.940
C	0.700	-9.117	0.215
H	1.056	-10.011	0.772
H	1.237	-9.084	-0.755
C	2.346	-7.780	1.245
H	2.920	-7.783	0.298
H	2.707	-8.638	1.851
C	2.570	-6.499	2.038
H	1.908	-6.550	2.914
H	3.616	-6.506	2.427
C	-4.127	-5.581	-0.706
H	-4.454	-6.505	-0.205
H	-5.013	-5.179	-1.248
C	-3.745	-4.587	0.383
H	-3.303	-3.663	-0.035
H	-4.670	-4.300	0.925
C	-2.718	-4.475	2.514
H	-3.589	-4.711	3.162
H	-2.711	-3.387	2.312
C	-1.441	-4.839	3.251
H	-1.430	-4.276	4.204
H	-1.416	-5.923	3.494

C	0.881	-4.241	3.141
H	1.067	-5.043	3.883
H	0.804	-3.289	3.702
C	2.037	-4.106	2.156
H	1.825	-3.242	1.507
H	2.946	-3.850	2.750

$\{[^{i}Pr_2NN_{F6}]Ni(\kappa^2\text{-}O_2N_2)\}^{1-}$

Ni	-0.107	-0.129	-0.191
O	-1.940	-0.158	-0.120
O	-0.330	-1.950	-0.267
N	-1.647	-2.336	-0.242
N	-2.466	-1.422	-0.169
N	1.833	-0.338	-0.201
N	-0.114	1.820	-0.131
F	0.307	4.594	0.884
F	4.644	-0.388	-1.141
F	4.893	1.601	-0.380
F	2.112	4.683	-0.276
F	4.577	-0.033	0.993
F	0.223	4.565	-1.283
C	4.194	0.460	-0.201
C	0.900	4.096	-0.217
C	-2.452	1.305	-3.066
C	1.097	-2.444	-3.283
C	3.603	-2.173	-3.559
C	-1.945	3.763	-3.409
C	3.031	-1.467	3.572
C	-1.119	2.042	2.604
C	-1.932	0.925	3.289

C	0.640	-2.134	3.042
C	-3.886	3.643	0.506
C	2.394	-1.909	-2.641
C	1.945	-1.526	2.483
C	-1.750	2.549	-2.482
C	2.291	2.041	-0.301
C	0.983	2.551	-0.212
C	2.584	-2.462	-1.227
C	3.001	-3.790	-1.059
C	2.666	0.685	-0.253
C	2.392	-2.269	1.224
C	2.309	-1.695	-0.068
C	-3.430	3.421	-0.794
C	-2.189	2.817	-1.041
C	-1.877	2.596	1.397
C	-1.401	2.440	0.072
C	-0.708	3.124	3.622
C	-3.115	3.223	1.588
C	3.140	-4.354	0.208
C	2.832	-3.596	1.335
H	3.483	-5.389	0.317
H	-3.491	3.374	2.606
H	2.918	-4.052	2.327
H	-0.672	2.325	-2.463
H	1.717	-0.487	2.196
H	2.280	-0.817	-2.560
H	-4.851	4.133	0.675
H	-0.139	-2.170	2.263

H	0.804	-3.164	3.412
H	0.266	-1.529	3.889
H	-2.843	1.328	3.771
H	-2.237	0.162	2.555
H	-1.325	0.435	4.075
H	-0.193	1.579	2.228
H	3.285	-2.472	3.959
H	3.958	-1.005	3.193
H	2.673	-0.868	4.431
H	-3.015	3.972	-3.597
H	-1.489	4.675	-2.988
H	-1.475	3.566	-4.391
H	4.541	-1.807	-3.109
H	3.092	2.765	-0.372
H	3.221	-4.398	-1.942
H	-4.055	3.728	-1.638
H	-0.087	3.907	3.156
H	-1.591	3.614	4.073
H	-0.126	2.669	4.446
H	3.729	-3.249	-3.779
H	3.463	-1.657	-4.527
H	-2.298	0.430	-2.415
H	-3.542	1.472	-3.159
H	-2.053	1.081	-4.074
H	1.159	-3.536	-3.455
H	0.232	-2.253	-2.627
H	0.924	-1.957	-4.262

14. References.

1. Haymore, B.; Feltham R. D. *Inorg. Chem.* **1973**, *14*, 81.
2. Carey, D. T.; Cope-Eatough, E. K.; Vilaplana-Mafe, E.; Mair, F. S.; Pritchard, R. G.; Warren, J. E.; Woods R. J. *Dalton Trans.* **2003**, 1083.
3. Kundu, S.; Stieber, S. C. E.; Ferrier, M. G.; Kozimor, S. A.; Bertke, J. A.; Warren, T. H. *Angew. Chem. Int. Ed.* **2016**, *55*, 10321.
4. Sakhaei, Z.; Kundu, S.; Donnelly, J. M.; Bertke, J. A.; Kim, W. Y.; Warren T. H. *Chem. Commun.* **2017**, *53*, 549.
5. Neese, F.; Zumft, W. G.; Antholine, W. E.; Kroneck, P. M. H. *J. Am. Chem. Soc.* **1996**, *118*, 8692.
6. (a) SHELXTL-PC, Vers. 5.10; 1998, Bruker-Analytical X-ray Services, Madison, WI.
7. Sheldrick, G. M. SHELX-97, Universität Göttingen, Göttingen, Germany.
8. Barbour, L. J. XSEED, 1999.
9. SADABS; Sheldrick, G. M. 1996, based on the method described in R. H. Blessing, *Acta Crystallogr. Sect. A*, **1995**, *51*, 33.
10. Ravel, B.; Newville, M. Athena, Artemis, Hephaestus: data analysis for X-ray absorption spectroscopy using IFEFFIT, *J. Synchrotron Rad.* **2005**, *12*, 537.
11. George, G. N. *EXAFSPAK, SSRL, SLAC; Stanford University: Stanford, CA, **2000**.*
12. Westre, T. E.; Kennepohl, P.; DeWitt, J. G.; Hedman, B.; Hodgson, K. O.; Solomon, E. I. *J. Am. Chem. Soc.* **1997**, *119*, 6297.
13. Neese, F. Orca: an ab initio, DFT and Semiempirical Electronic Structure Package, Version 3.0.3; Max Planck Institute for Chemical Energy Conversion; Mülheim an der Ruhr, Germany.
14. Stieber, S. C. E.; Milsmann, C.; Hoyt, J. M.; Turner, Z. R.; Finkelstein, K. D.; Wieghardt, K.; DeBeer, S.; Chirik, P. J. *Inorg. Chem.* **2012**, *51*, 3770.
15. Towns, J.; Cockerill, T.; Dahan, M.; Foster, I.; Gaither, K.; Grimshaw, A.; Hazlewood, V.; Lathrop, S.; Lifka, D.; Peterson, G. D.; Roskies, R.; Ray Scott, J.; Wilkins-Diehr, N. *Comput. Sci. Eng.* **2014**, *16*, 62.
16. Perdew, J. P. *Phys. Rev. B* **1989**, *33*, 8822.
17. Perdew, J. P. *Phys. Rev. B* **1986**, *34*, 7406.
18. Lee, C. T.; Yang, W. T.; Parr, R. G. *Phys. Rev. B* **1988**, *37*, 785.

19. Neese, F.; Solomon, E. I. In Magnetism: From Molecules to Materials; Miller, J. S., Drillon, M., Eds.; Wiley: New York, **2002**; Vol. 4, p 345.
20. Schäfer, A.; Horn, H.; Ahlrichs, R. *J. Chem. Phys.* **1992**, *97*, 2571.
21. Schäfer, A.; Huber, C.; Ahlrichs, R. *J. Chem. Phys.* **1994**, *100*, 5829.
22. Weigend, F.; Ahlrichs, R. *Phys. Chem. Chem. Phys.* **2005**, *7*, 3297.
23. Eichkorn, K.; Weigend, F.; Treutler, O.; Ahlrichs, R. *Theor. Chem. Acc.* **1997**, *97*, 119.
24. Eichkorn, K.; Treutler, O.; Öhm, H.; Häser, M.; Ahlrichs, R. *Chem. Phys. Lett.* **1995**, *240*, 283.
25. Eichkorn, K.; Treutler, O.; Öhm, H.; Häser, M.; Ahlrichs, R. *Chem. Phys. Lett.* **1995**, *242*, 652.
26. Neese, F.; Wennmohs, F.; Hansen, A.; Becker, U. *Chem. Phys.* **2009**, *356*, 98.
27. Kossmann, S.; Neese, F. *Chem. Phys. Lett.* **2009**, *481*, 240.
28. Neese, F. *J. Comput. Chem.* **2003**, *24*, 1740.
29. Ginsberg, A. P. *J. Am. Chem. Soc.* **1980**, *102*, 111.
30. Noodleman, L.; Peng, C. Y.; Case, D. A.; Mouesca, J. M. *Coord. Chem. Rev.***1995**, *144*, 199.
31. Kirchner, B.; Wennmohs, F.; Yes, S.; Neese, F. *Curr. Opin. Chem. Biol.* **2007**, *11*, 134.
32. Pettersen, E. F.; Goddard, T. D.; Huang, C. C.; Couch, G. S.; Greenblatt, D. M.; Meng, E. C.; Ferrin, T. C. *J. Comput. Chem.* **2004**, *13*, 1605.
33. Kirchner, B.; Wennmohs, F.; Yes, S.; Neese, F. *Curr. Opin. Chem. Biol.* **2007**, *11*, 134.
34. Schaefer, A.; Horn, H.; Ahlrichs, R. *J. Chem. Phys.* **1992**, *97*, 2571.
35. ftp.chemie.uni-karlsruhe.de/pub/basen
36. Sinnecker, S.; Slep, L. D.; Bill, E.; Neese, F. *Inorg. Chem.* **2005**, *44*, 2245.
37. DeBeer George, S.; Petrenko, T.; Neese, F. *J. Phys. Chem. A* **2008**, *112*, 12936.